NASA TECHNICAL NOTE

NASA TN D-7449

NASA TN D-7449

FORE-AND-AFT ELASTIC RESPONSE CHARACTERISTICS OF 34 × 9.9, TYPE VII, 14 PLY-RATING AIRCRAFT TIRES OF BIAS-PLY, BIAS-BELTED, AND RADIAL-BELTED DESIGN

by John A. Tanner

Langley Research Center
Hampton, Va. 23665

NATIONAL AERONAUTICS AND SPACE ADMINISTRATION • WASHINGTON, D. C. • APRIL 1974

FORE-AND-AFT ELASTIC RESPONSE CHARACTERISTICS OF 34 × 9.9, TYPE VII, 14 PLY-RATING AIRCRAFT TIRES OF BIAS-PLY, BIAS-BELTED, AND RADIAL-BELTED DESIGN*

By John A. Tanner
Langley Research Center

SUMMARY

An investigation was conducted to determine the fore-and-aft elastic response characteristics of 34 × 9.9, type VII, 14 ply-rating aircraft tires of bias-ply, bias-belted, and radial-belted design. The investigation consisted of static and rolling tests on dry concrete pavements at the Langley aircraft landing loads and traction facility; statistical techniques which related the measured tire elastic characteristics to variations in the vertical load, inflation pressure, braking force and/or tire vertical deflection; and a semiempirical analysis which related the tire elastic behavior to measured wheel slippage during steady-state braking.

The bias-belted tire developed the largest spring constant value for most loading conditions; the radial-belted tire, the smallest. The elastic response of the tire free periphery to static braking included both tread stretch and carcass torsional wind-up about the axle for the bias-ply and bias-belted tires and carcass wind-up alone for the radial-belted tire. Similarly, tread stretching under braked rolling conditions was detected within the footprints of the bias-ply and bias-belted tires but not within the footprint of the radial-belted tire. The tire slippage during steady-state braking was greater for the bias-ply tire than for the bias-belted and radial-belted tires.

INTRODUCTION

The most costly maintenance item associated with aircraft landing gear systems is the replacement of worn or damaged aircraft tires (ref. 1). One of the more promising approaches to increased tread life, which has proven successful in automotive applications, is to replace conventional bias-ply tires with either bias-belted or radial-belted tires. This approach could also result in an improvement in the cornering and braking traction

---

*The information presented herein was offered as a thesis in partial fulfillment of the requirements for the degree of Master of Science, George Washington University, May 1973.

available to the aircraft if the belted carcass design reduces tire scrubbing and associated heat generation within the footprint during ground maneuver operations as advertised by tire manufacturers. However, since the bias-belted and radial-belted designs differ from that of the conventional bias-ply tire, it is reasonable to speculate that the elastic response characteristics of these tires will also differ.

In 1965, reference 2 presented the results of an analog computer model study which indicated that the braking performance of aircraft antiskid braking systems, which produced a cyclic braking effort, could be affected by the elastic response characteristics of aircraft tires in the fore-and-aft or braking direction. The results of this computer study were later corroborated by experimental data (ref. 3). In their operation, antiskid systems control the application of brake torque by sensing wheel angular velocity and/or acceleration. However, because of the elastic behavior of the tire, the angular velocity and acceleration of the wheel can differ significantly from that of the tire, particularly at the tire-pavement interface where the braking traction is actually developed. This flexibility between the wheel and the pavement influences the operational behavior of the antiskid braking systems. Therefore a knowledge of the fore-and-aft elastic response characteristics of aircraft tires is necessary if improvements in economical operations and safety of aircraft antiskid braking systems are to be made.

References 4 to 11 are examples of early (1940-1958) research papers which studied tire elastic response characteristics. These early studies dealt primarily with tire lateral deformations since wheel shimmy was a serious problem in the automotive and aircraft industries, and sophisticated aircraft antiskid systems were still years away from development. In 1965, when reference 2 was published, the information on tire fore-and-aft elastic response characteristics was limited to a few static data points (ref. 12) and an empirical analysis (ref. 13) based entirely upon the free peripheral measurements presented in reference 12. Reference 14, published in 1971, studied the fore-and-aft elastic response characteristics of bias-ply aircraft tires in more detail, but no data are available which describe the fore-and-aft elastic response characteristics of bias-belted and radial-belted aircraft tires.

The purpose of this paper is to present the results of an investigation to determine the fore-and-aft elastic response characteristics of 34 × 9.9, type VII, 14 ply-rating aircraft tires of bias-ply, bias-belted, and radial-belted construction. These characteristics, which include fore-and-aft spring constant, fore-and-aft decay length along the free periphery, and deformation variation within the rolling footprint, were obtained over a range of vertical loads from 51.2 kN (11 500 lb) to 66.8 kN (15 000 lb) and inflation pressures from 621 kPa (90 lb/in^2) to 965 kPa (140 lb/in^2) at ground speeds up to 100 knots (1 knot = 0.514 m/sec) and at braking forces up to 22.2 kN (5000 lb). The investigation consisted of static and rolling tests on dry concrete surfaces at the Langley

landing loads and traction facility. Statistical techniques were used to relate the measured tire elastic characteristics to variations in the vertical load, inflation pressure, braking force, and/or tire vertical deflection, and a semiempirical analysis was used to relate tire elastic behavior to measured wheel slippage during study-state braking.

The tires used in the tests were supplied by the U.S. Air Force under task number AFAN-625.

SYMBOLS

Values are given in both SI and U.S. Customary Units. The measurements and calculations were made in U.S. Customary Units. Factors relating the two systems are given in reference 15.

a,b	displacements
C	tire circumference
F_x	braking force
F_z	vertical load
h	footprint half-length
J	decay length
K_x	static fore-and-aft spring constant
l	distance
M	rolling footprint deformation variation, $M = \frac{m}{u_{f0}}$
m	linear slope
N	number of wheel revolutions
p	inflation pressure
Q	tread stretch

R	rolling radius
r, r^2	statistical correlation coefficients
s	tire circumferential distance
u	deformation
x_t	total tire slippage
$\alpha, \beta, \gamma, \eta$	generalized constants
δ	tire vertical deflection
ΔR	change in rolling radius
ϵ_x	elongation strain due to braking
μ	coefficient of friction

Subscripts:

b	braked
calc	calculated
exp	experimental
f	footprint
f_0	center of footprint
max	maximum value
o	unbraked
p	free periphery
p_i	peripheral station

p_0 footprint leading edge

t total

x fore-and-aft

APPARATUS AND TEST PROCEDURE

Test Tires

The tires of this investigation were 34 × 9.9, type VII, 14 ply-rating aircraft tires of bias-ply, bias-belted, and radial-belted design. Figure 1 is a photograph of the tires before testing and the shape of the tire footprint under rolling conditions is shown in figure 2. The differences in tire construction are illustrated by the sketches in figure 3. The bias-ply tire is constructed with the carcass plies arranged on a bias to form a relative angle between the reinforcing cords of alternating plies. The carcass is then capped with the tire tread. The bias-belted tire is constructed in the same manner as the bias-ply tire except that a circumferential reinforcing belt is added to the carcass. The radial-belted tire is constructed with the reinforcing cords of the carcass plies oriented radially about the tire. The carcass of this tire is then reinforced with a circumferential belt and capped with the tire tread. Specifications for the three tires are presented in table I.

Test Facility

In its present configuration, the Langley aircraft landing loads and traction facility (formerly called the Langley landing-loads track) consists of a rail system 671 m (2200 ft) long by 9.2 m (30 ft) wide, a large hydraulically operated water-jet catapult system, an arresting system, and two test carriages. A schematic of the facility is presented in figure 4 and an aerial photograph is shown in figure 5. The central feature of the catapult system is an L-shaped pressure vessel containing 37.8 m^3 (10 000 gal) of water. This vessel is pressurized with air, up to 22.1 MPa (3200 lb/in^2), and a timed, quick-acting valve at the front of the vessel releases a high energy jet of water, through a 17.78-cm-diameter (7 in.) nozzle, which impinges upon a U-shaped turning bucket at the rear of the test carriage. The catapult can develop approximately 2000 kN (450 000 lb) of thrust which is sufficient to accelerate either test carriage to speeds of 120 knots in 2.5 to 3 sec over about 122 m (400 ft). After accelerating to the desired speed, the test carriage coasts through the test section of the facility, about 366 m (1200 ft), and is brought to a stop by 5 parallel arresting cables which are interconnected to 20 arresting gear engines.

Both the static and rolling tests were conducted with the wheel, tire, and brake assembly mounted in an instrumented yoke dynamometer which was attached to the center drop frame of the large test carriage. This carriage, shown in figure 6, weighs approximately 54 431 kg (120 000 lbm). The dead weight of the drop frame was 5205 kg (11 500 lbm) and was down-loaded hydraulically to increase the tire vertical loadings. For the tests described in this paper, the test runway had a concrete surface with a light broom finish. The average texture depth was 0.0787 mm (0.0031 in.) which was somewhat smoother than those of most operational runways. A camera pit was installed in the test runway at its midpoint and covered with a glass plate, 229 cm (90 in.) long by 122 cm (48 in.) wide by 20 cm (8 in.) thick, which was mounted flush with the concrete surface. This glass plate can withstand a 178 kN (40 000 lb) load at its midspan. The glass plate was cleaned and dried before each test, and the braking forces developed on its surface were comparable to those developed on the concrete surface.

Static Tests

The objectives of the static tests were to determine the tire fore-and-aft spring constants and to measure the deformation or stretch along the free periphery. Two different test procedures were required to meet these objectives and each is described separately in the paragraphs which follow.

Spring constants.- Figure 7 is a photograph of the static test equipment employed to determine the fore-and-aft spring constants of the test tires. This equipment consisted of the test tire, which rested under a vertical load on the surface of a bearing plate, and the instrumentation necessary to monitor the tire loadings and the bearing-plate displacements. The carriage and wheel were externally braced to prevent axle translation and wheel rotation. Tire loadings included the vertical load which was controlled by the carriage hydraulic system and the fore-and-aft, or static braking, force which was applied to the bearing plate by means of a hydraulic piston. The magnitude of the vertical load applied to the tire was measured by load cells under the bearing plate, and the braking force was measured by a load cell located between the hydraulic piston and the backstop. The braking forces were restricted to levels insufficient to produce any discernible slippage in the tire—bearing-plate interface. Fore-and-aft displacements of the bearing plate during brake force applications were obtained from a dial gage. Since there was no relative motion (no slippage) between the tire footprint and the bearing plate, those bearing-plate displacements correspond to the footprint displacements with respect to the axle. The testing technique involved the application of the desired vertical load to the tire, the incremental application of braking force, and the recording of the resulting displacements of the footprint with respect to the axle.

Deformation in the free periphery.- Deformations in the free periphery were measured concurrently with the spring constants. In preparation for these measurements, a

number of cone-shaped rubber studs were attached along the periphery of each tire as shown in figure 7 and a camera was mounted to a beam which was free to rotate about the axle center line. Free periphery deformations were obtained from projected enlargements of photographs taken of the studs during the course of the static tests.

Rolling Tests

The objectives of the braked- and unbraked-rolling tests were to measure the deformation or stretch within the footprint and to determine the braked and unbraked apparent tire rolling radii. Two different test procedures were required to meet these objectives and each is described separately.

Deformation within the footprint.- Figure 8 is a photograph of the carriage during the tests to determine the deformation within the rolling footprint. The deformations resulting from the combined vertical and braking forces on the tire were determined from projected enlargements of photographs of the tire footprint taken through the glass plate installed in the runway. In preparation for these tests, equally spaced small holes 3.2 mm (1/8 in.) in diameter and 1.6 mm (1/16 in.) deep were drilled along the tread periphery and filled with a white silicone rubber as shown in figure 2. The test procedure involved rolling the tire, under the desired vertical load, over the glass plate at a speed of approximately 5 knots. The brake pressure was preset at values which were sufficient to develop the desired braking force but incapable of producing a locked-wheel skid; photographs were taken of the passing footprint.

Braked and unbraked tire rolling radii.- These tests were conducted on the dry concrete runway at the desired vertical loads, inflation pressures, and braking forces. The test procedure involved towing or catapulting the carriage to the desired speed, applying the desired loads, and recording the load and displacement data as time histories on an oscillograph. Measurements of the vertical load and braking force were obtained from the instrumented dynamometer, and the braked and unbraked apparent tire rolling radii were determined from measurements of the distance traveled along the runway and the total number of wheel revolutions.

Statistical Techniques

Statistical analysis techniques were used to establish linear relationships between the tire fore-and-aft elastic response characteristics and the loading parameters. Three different techniques were used in this investigation and each is briefly noted.

Method of least squares.- When a relationship between two variables was needed, the method of least squares (ref. 16) was used to determine the best unbiased estimate of the linear relationship and to define the correlation coefficient.

Multiple regression analysis.- When a relationship between tire fore-and-aft elastic response characteristics and several loading parameters was needed, a multiple regression analysis (ref. 17) was performed to determine the matrix of coefficients and to define the degree of correlation.

Analysis of variance rationale.- When it was necessary to determine which loading parameters had a significant effect on the tire fore-and-aft elastic response characteristics, the analysis of variance rationale (ref. 18) was used to construct an ANOVA table, and a test for significance based on the F distribution table (ref. 18) was performed.

RESULTS AND DISCUSSION

Force and displacement measurements on bias-ply, bias-belted, and radial-belted aircraft tires were obtained under both static and rolling conditions. The measurements under static conditions were used to define the tire fore-and-aft spring constant and to establish the tread-stretch distribution due to the braking effort along the free periphery near the footprint leading edge. The measurements under rolling conditions were used to establish the tread-stretch distribution within the leading portion of the footprint and the apparent change in rolling radius due to the braking effort. The following sections discuss the variation of these tire elastic characteristics with vertical load, tire vertical deflection, inflation pressure, and braking force and include a discussion of variations in the tire rolling radius and their effect on both wheel and tire slippages.

Static Response

Fore-and-aft spring constant.- The fore-and-aft spring constant K_x is a fundamental characteristic which defines the elastic deformation of the tire when subjected to a braking force. This spring constant takes into account both the circumferential deformation of the tread and the torsional wind-up of the carcass resulting from brake application and is therefore a measure of the overall elastic response of the braked tire. It was obtained experimentally for each tire under various vertical loads and inflation pressures by relating the braking force to the footprint deformation with respect to the axle.

Typical fore-and-aft load-deflection data for bias-ply, bias-belted, and radial-belted tires under static loading conditions are presented in figure 9. These data were obtained over one and one-half loading cycles to establish the complete hysteresis loops. The value of K_x was taken as the slope of the line which connected the end points of each loop. Spring constants and static vertical deflection data for each tire are presented in table II.

The variation of K_x with tire vertical deflection is shown in figure 10. The linear curves fairing the data in the figure were obtained by the least-squares method and are

represented by the following equations:

Bias-ply tires:

$$\left.\begin{aligned} K_x &= 1.6\ \text{MN/m} - (8.6\ \text{MPa})\delta \\ K_x &= 9276\ \text{lb/in.} - (1254\ \text{lb/in}^2)\delta \end{aligned}\right\} \quad (1)$$

with $r = -0.82$

Bias-belted tires:

$$\left.\begin{aligned} K_x &= 1.9\ \text{MN/m} - (11.4\ \text{MPa})\delta \\ K_x &= 10\ 995\ \text{lb/in.} - (1650\ \text{lb/in}^2)\delta \end{aligned}\right\} \quad (2)$$

with $r = -0.93$

Radial-belted tires:

$$\left.\begin{aligned} K_x &= 1.3\ \text{MN/m} - (6.4\ \text{MPa})\delta \\ K_x &= 7476\ \text{lb/in.} - (934\ \text{lb/in}^2)\delta \end{aligned}\right\} \quad (3)$$

with $r = -0.84$

For these equations, δ is measured in m (in.).

The magnitude of r is a measure of the correlation between the data and the faired curves (±1.00 represents perfect agreement), and the sign of r is determined by the slope of the faired curves. The data presented in figure 10 indicate that K_x decreases with vertical deflection for all three tires over the test range of vertical deflections. The bias-belted tire has the highest values of K_x for a given tire deflection followed in order by the bias-ply and radial-belted tires. Furthermore, the bias-belted tire has the sharpest decrease in K_x with vertical load followed in order by the bias-ply and radial-belted tires. The values of K_x for the bias-ply tire presented in figure 10 are within 15 percent of the values calculated from equation (47) of reference 13.

In an effort to obtain further insight into the variation of the data presented in table II, a multiple regression analysis was performed to investigate the influence on K_x of variations in the vertical load and inflation pressure. This analysis assumed a linear

relationship over the test range of parameters and yielded the following set of equations:

Bias-ply tires:

$$\left.\begin{aligned} K_x &= 313\ \text{kN/m} + (1.26\ \text{m}^{-1})F_z + (0.86\ \text{m})p \\ K_x &= 1788\ \text{lb/in.} + (0.0320\ \text{in}^{-1})F_z + (33.84\ \text{in.})p \end{aligned}\right\} \quad (4)$$

with $r^2 \approx 1.00$

Bias-belted tires:

$$\left.\begin{aligned} K_x &= 693\ \text{kN/m} - (4.36\ \text{m}^{-1})F_z + (0.90\ \text{m})p \\ K_x &= 3956\ \text{lb/in.} - (0.1108\ \text{in}^{-1})F_z + (35.35\ \text{in.})p \end{aligned}\right\} \quad (5)$$

with $r^2 \approx 1.00$

Radial-belted tires:

$$\left.\begin{aligned} K_x &= 719\ \text{kN/m} - (5.33\ \text{m}^{-1})F_z + (0.51\ \text{m})p \\ K_x &= 4106\ \text{lb/in.} - (0.1354\ \text{in}^{-1})F_z + (19.94\ \text{in.})p \end{aligned}\right\} \quad (6)$$

with $r^2 \approx 1.00$

For these equations, F_z is measured in N (lb) and p is measured in Pa (lb/in^2).

The magnitude of r^2, which is a measure of the ability of the equations to fair the data, may be artificially high for equations (4) to (6) since only nine data points were used to develop each equation.

The equation for the bias-ply tire (eq. (4)) indicates that K_x increases with the vertical load thereby corroborating the results for constant pressure presented in reference 14. However, the equations for bias-belted and radial-belted tires (eqs. (5) and (6)) indicate that K_x decreases with vertical load for constant pressure. All three equations indicate that the fore-and-aft spring constant increases with the inflation pressure for a constant vertical load and differs from the pressure trends noted in reference 13.

Free periphery deformation distribution.- Experimental tests were performed to investigate the variation of tread deformation along the free periphery of each tire under static loading conditions. A schematic representation of this deformation is presented

in figure 11. As in references 13 and 14, the footprint was assumed to deform as a unit for these tests, that is, no localized stretching within the static footprint. Further, maximum tire deformation was assumed to occur at the leading edge of the footprint; therefore, during brake application the deformation at this point, identified as u_{p0} in figure 11(b), is defined by the ratio F_x/K_x. The deformations at other points along the free periphery (u_{pi} in the figure) were obtained by subtracting from the maximum deformation the stretch accumulated between the leading edge of the footprint and the point in question.

A sample of the results from these tests is presented in figure 12 where the deformations are plotted (on a logarithmic scale) as a function of circumferential distance from the footprint leading edge (on a linear scale). The deformations for the bias-ply and bias-belted tires are shown initially to decay linearly from their maximum values as the circumferential distance from the footprint leading edge s_p increases and then to remain essentially unchanged with a further increase in s_p. The deformations for the radial-belted tires are shown to remain constant regardless of the distance from the footprint leading edge; this result implies no tread stretch due to the braking effort.

The data presented in figure 12 indicate that the elastic response of the bias-ply and bias-belted tires to static braking forces includes both tread stretch in the immediate vicinity of the footprint and torsional deformation of the tire carcass about the axle. The elastic response of the radial-belted tire to static braking forces is observed to be strictly a torsional deformation of the carcass about the axle (no tread stretch). The linearity of the data for all three tires in the region near the footprint leading edge suggests an exponential relationship in that region between the tread deformation and the circumferential distance from the footprint leading edge. This relationship is expressed as follows:

$$u_p = \frac{F_x}{K_x} e^{-s_p/J_x} \qquad \left(0 \geqq s_p \geqq s_{p,max}\right) \tag{7}$$

where $s_{p,max}$ is the distance from the footprint leading edge to the point where the deformation attains a constant level. The slope of the exponential curve is defined as $-1/J_x$ where J_x is referred to as the decay length and is a fundamental tire elastic characteristic which defines the deformation distribution along the free periphery (the smaller the value of J_x, the greater the tread stretch in the tire free periphery).

A quantitative measure of the tire deformation along the free periphery was obtained by choosing an appropriate value of $s_{p,max}$ and by using the least-squares method to compute J_x for each tire at various vertical loads, inflation pressures, and braking forces. In order to simplify these computations, $s_{p,max}$ was set equal to 35.6 cm (14 in.) which was observed to be the maximum value of $s_{p,max}$ for either the bias-ply

or bias-belted tires. By eliminating $s_{p,max}$ as a variable, the computed values of J_X now become a direct measure of the tread-stretch contribution to the total tire elastic response to the braking force (the smaller the value of J_X, the larger the tread-stretch contribution). However, this technique also causes the computed values of J_X to be artificially high for the bias-ply and bias-belted tires under several loading conditions. These values of decay length J_X are presented in table III. The data indicate that J_X for the bias-ply and bias-belted tires may be a function of the loading conditions, but J_X for the radial-belted tire approaches infinite values for all loading conditions.

In order to obtain additional information on the variation of J_X with loading conditions for the bias-ply and bias-belted tires, a 3^3 factorial ANOVA table (ref. 18) was constructed for the bias-ply data presented in table III. The results of the tests based on the ANOVA table indicated (with a 90-percent confidence) that J_X for the bias-ply tire was sensitive to variations in inflation pressure and braking force and was insensitive to variations in the vertical load when $s_{p,max}$ was set at 35.6 cm (14 in.). This variation of J_X with braking force is contrary to the results presented in reference 14 where the decay length was essentially independent of the braking force. On the basis of the ANOVA table results, the equations which expressed J_X for the bias-ply and bias-belted tires were assumed to be of the form

$$J_X = \alpha + \eta F_X + \gamma p \tag{8}$$

over the test range of parameters.

A multiple regression analysis based on equation (8) produced the following relationships:

Bias-ply tires:

$$\left.\begin{aligned} J_X &= 0.8903\ \text{m} - (0.0422\ \text{m/N})F_X + (0.505\ \mu\text{m}^3/\text{N})p \\ J_X &= 35.05\ \text{in.} - (0.0074\ \text{in./lb})F_X + (0.1371\ \text{in}^3/\text{lb})p \end{aligned}\right\} \tag{9}$$

with $r^2 = 0.890$

Bias-belted tires:

$$\left.\begin{aligned} J_X &= 1.289\ \text{m} - (0.0336\ \text{m/N})F_X - (0.122\ \mu\text{m}^3/\text{N})p \\ J_X &= 50.78\ \text{in.} - (0.0059\ \text{in./lb})F_X - (0.0332\ \text{in}^3/\text{lb})p \end{aligned}\right\} \tag{10}$$

with $r^2 = 0.800$

For these equations, F_X is measured in N (lb) and p is measured in Pa (lb/in^2). Equation (9) indicates that J_X for the bias-ply tire decreases with the braking force and increases with the inflation pressure. Equation (10) indicates that J_X for the bias-belted tire decreases with either the braking force or the inflation pressure. A comparison of the two equations shows that the decay lengths for the bias-belted tire are generally higher than those for the bias-ply tire for most loading conditions.

Rolling Response

Deformation within the footprint.- The circumferential deformation in the leading half of the rolling footprint during brake application was studied under low-speed conditions (≈5 knots). Typical data from these tests obtained under loading conditions comparable to those of the static tests are presented in figure 13. The deformation at the geometrical center of the footprint, which was observed to be the point of maximum deformation for the bias-ply and bias-belted tires, was set equal to F_X/K_X, and the deformation at other points within the leading half of the footprint were obtained by subtracting from F_X/K_X the tire deformation accumulated between the center of the footprint and the point in question. The values of K_X for each tire were calculated from equations (4), (5), and (6). The data presented in figure 13 indicate that, under braking conditions, stretching occurs in the footprint of the bias-ply and bias-belted tires but, as observed in the free peripheral measurements, not in the footprint of the radial-belted tire. The tread deformations for the bias-ply and bias-belted tires were observed to vary linearly within the rolling footprint.

A numerical measure of this deformation was obtained by multiplying the displacements by K_X/F_X to normalize the data and by using the least-squares method to compute the slope M of the normalized footprint data for each tire under various loading conditions. These data are presented in table IV. The variation of tread deformation with loading conditions was determined for the bias-ply and bias-belted tires by assuming an equation for the slope to be of the form

$$M = \alpha + \eta F_X + \beta F_Z + \gamma p \tag{11}$$

for the test range of parameters.

A multiple regression analysis of the data presented in table IV yielded the following equations:

Bias-ply tires:

$$\left.\begin{aligned} M &= -1.031\ m^{-1} - \left[1.309 \times 10^{-4}\ (N\text{-}m)^{-1}\right]F_X + \left[4.9 \times 10^{-5}\ (N\text{-}m)^{-1}\right]F_Z \\ &\quad - (3.8081 \times 10^{-6}\ m/N)p \\ M &= -2.620 \times 10^{-2}\ in^{-1} - \left[1.48 \times 10^{-5}\ (lb\text{-}in.)^{-1}\right]F_X \\ &\quad + \left[5.538 \times 10^{-6}\ (lb\text{-}in.)^{-1}\right]F_Z - (6.669 \times 10^{-4}\ in./lb)p \end{aligned}\right\} \quad (12)$$

with $r^2 = 0.988$

Bias-belted tires:

$$\left.\begin{aligned} M &= -3.326\ (m^{-1}) - \left[4.211 \times 10^{-5}\ (N\text{-}m)^{-1}\right]F_X + \left[3.397 \times 10^{-5}\ (N\text{-}m)^{-1}\right]F_Z \\ &\quad - (1.259 \times 10^{-6}\ m/N)p \\ M &= -8.447 \times 10^{-2}\ in^{-1} - \left[4.758 \times 10^{-6}\ (lb\text{-}in.)^{-1}\right]F_X \\ &\quad + \left[3.839 \times 10^{-6}\ (lb\text{-}in.)^{-1}\right]F_Z - (2.206 \times 10^{-4}\ in./lb)p \end{aligned}\right\} \quad (13)$$

with $r^2 = 0.976$

For these equations, F_X and F_Z are measured in N (lb) and p is measured in Pa (lb/in^2).

Equations (12) and (13) indicate that the magnitude of M for both tires increases with the braking force and inflation pressure and decreases with the vertical load.

Rolling radius calculations.- The tire deformation data presented in this paper suggest that the elastic response of these aircraft tires to braking forces can be described in terms of tread stretch and/or torsional wind-up of the tire carcass about the axle. That portion of the tire elastic response which is attributed to tread stretch would be reflected in changes in the tire rolling radius during steady-state brake applications. Therefore, it is appropriate to develop an equation which expresses the change in rolling radius in terms of previously defined tire elastic properties. This equation, derived in the appendix, is

$$\Delta R = \frac{Q_t}{2\pi} = \frac{F_X}{2\pi K_X}\left[1 - (1 + Mh)e^{-s_{p,max}/J_X}\right] \quad (14)$$

This general expression may be used to compute the change in rolling radius due to braking regardless of the tire construction. However, equation (14) is considerably

different from the expressions for computing ΔR which were developed in references 13 and 14, where ΔR was equated to the product of the tire unloaded radius and the maximum value of the circumferential strain of the tread. Furthermore, on the basis of the analysis presented in the appendix, the expressions for computing ΔR presented in references 13 and 14 appear to be in error and would overestimate the net change in the tire rolling radius by a factor of 2π.

Application of Results

Apparent change in rolling radius.- Experimental braked- and unbraked-rolling tests were conducted to determine the apparent change in rolling radius (or wheel slippage) of the bias-ply, bias-belted, and radial-belted tires under various loading conditions. For each tire, the apparent rolling radius R_b or R_o was determined by relating the distance traveled l to the number of wheel revolutions N as follows:

$$R_b \text{ or } R_o = \frac{l}{2\pi N} \tag{15}$$

The experimental change in rolling radius is the difference between the apparent rolling radii of the braked and the freely rolling tire and is given as follows:

$$\Delta R_{exp} = R_b - R_o \tag{16}$$

When computed in this manner, ΔR_{exp} includes both the effective change in rolling radius due to tire slippage within the tire-pavement interface and the actual change in rolling radius due to the elastic deformation of the tire tread.

Values of ΔR_{exp} for each tire are presented in table V. The calculated values of change in rolling radius ΔR_{calc}, also presented in table V, are based upon equation (14) and consider only the effect of tire stretch. For the purpose of these calculations the values of K_x, J_x, and M for the bias-ply and bias-belted tires were computed from equations (4) and (5), (9) and (10), and (12) and (13), respectively. For the radial-belted tire, the values of K_x were computed from equation (6) and the values of J_x and M were equal to ∞ and 0, respectively. The footprint half-lengths were obtained from table IV and the value of $s_{p,max}$ was set equal to 35.6 cm (14 in.) for all test conditions. The changes in rolling radius during braking as calculated from equation (14) are compared in figure 14 with those obtained experimentally. The tire slip boundary is defined by the straight line near the left edge of the figure and is the line of agreement between calculated and experimental values of ΔR. The data indicate that a major portion of the apparent change in rolling radius of the bias-ply and bias-belted tires and virtually all

the apparent change in rolling radius of the radial-belted tire measured experimentally are due to an actual tire slippage within the tire-pavement interface.

Tire slip ratio.- Once the actual change in rolling radius due to tire elastic deformation has been established, the tire slip ratio can be determined from the following equation:

$$\frac{x_t}{C} = \frac{2\pi}{C}\left(\Delta R_{exp} - \Delta R_{calc}\right) \tag{17}$$

The ratio x_t/C is the tire slip ratio, where x_t is the tire skidding distance per wheel revolution and C is the unloaded tire circumference. The braking force friction coefficient μ_x is a measure of the braking effort and is defined as

$$\mu_x = \frac{F_x}{F_z} \tag{18}$$

The variation of μ_x with tire slip ratio for the three tire designs is presented in figure 15 where the values of μ_x and x_t/C were computed from the data presented in table V. The equations for the faired curves in the figure were determined by the least-squares method and are given as follows:

Bias-ply tires:

$$\mu_x = 0.038 + 6.373\,\frac{x_t}{C} \tag{19}$$

with $r = 0.88$

Bias-belted tires:

$$\mu_x = 0.031 + 8.913\,\frac{x_t}{C} \tag{20}$$

with $r = 0.75$

Radial-belted tires:

$$\mu_x = -0.071 + 42.017\,\frac{x_t}{C} \tag{21}$$

with $r = 0.40$

The small value of r for the radial-belted data is the result of the nearly vertical slope of the faired curve (fig. 15) rather than the lack of data correlation. These data indicate that for a given steady-state braking level, or μ_x, the bias-ply tire is subjected to the

most severe tire slippage and the radial-belted tire to the least. The slippage associated with the bias-belted tire is only slightly less than that of the bias-ply tire.

CONCLUDING REMARKS

Tests were conducted to determine the fore-and-aft elastic response characteristics of 34 × 9.9, type VII, 14 ply-rating aircraft tires of bias-ply, bias-belted, and radial-belted design. These characteristics, which include the static fore-and aft spring constant, fore-and-aft decay length along the free periphery, and deformation variation within the rolling footprint, were obtained over a range of vertical loads and inflation pressures at ground speeds up to 100 knots and at braking forces up to 22.2 kN (5000 lb). The investigation consisted of static and rolling tests on dry concrete pavements at the Langley aircraft landing loads and traction facility, statistical techniques which related the measured tire elastic characteristics to variations in the vertical load, inflation pressure, braking force, and/or tire vertical deflection, and a semiempirical analysis which related tire elastic behavior to measured wheel slippage during steady-state braking.

The bias-belted tire had the largest spring constant for most loading conditions; the radial-belted tire, the smallest. The static fore-and-aft spring constant (1) decreased with tire vertical deflection and increased with inflation pressure for each of the three tires and (2) increased with vertical load for the bias-ply tire and decreased with vertical load for the bias-belted and radial-belted tires.

The elastic response of the tire free periphery to static braking included both tread stretch and carcass torsional wind-up about the axle for the bias-ply and bias-belted tires and carcass wind-up alone for the radial-belted tire. The decay lengths for the bias-belted tire were longer than those for the bias-ply tire for most loading conditions, whereas the decay lengths for the radial-belted tire approached infinity and, as a result, the lack of tread stretch was noted during brake application. The fore-and-aft decay length (1) was insensitive to variations in the vertical load for the bias-ply tire and decreased with braking force for both the bias-ply and bias-belted tires and (2) increased with inflation pressure for the bias-ply tire and decreased with inflation pressure for the bias-belted tire.

Tread stretching under braked-rolling conditions was detected within the footprints of the bias-ply and bias-belted tires and was found to increase with braking force and inflation pressure and to decrease with vertical load. No tread stretching was detected within the footprint of the radial-belted tire.

The tread-stretch contribution to changes in rolling radius due to braking can be predicted from the elastic fore-and-aft response characteristics of the tires. These changes in rolling radius, based upon the tire elastic deformation measurements, can then be used in conjunction with the experimentally determined wheel response characteristics to calculate the actual tire slippage under steady-state braked-rolling conditions. Tire slippage during steady-state braking was less for radial-belted tires than for those of bias construction.

The results of this investigation have several implications which are of interest to designers of aircraft landing gears and antiskid braking systems. The extent of tire slippage and hence scrubbing action associated with the three tire designs implies higher wear rates during braking operations for the bias-ply tire and, to a slightly lesser extent, the bias-belted tire than for the radial-belted tire. In addition, the reduced tire slippages noted particularly for the radial-belted tire design could also result in lower tread temperatures during high-speed operations which would suggest improved traction performance. However, the low fore-and-aft spring stiffness of the radial-belted tire could introduce an excessive lag between the braking effort and the ground reaction which would alter the response characteristics of the aircraft antiskid braking system sufficiently to degrade its performance. Hence, designers of landing gears and antiskid braking systems must weigh the possible advantages of belted designs (tire wear and traction improvements) against this possible degradation in antiskid braking performance.

Langley Research Center,
National Aeronautics and Space Administration,
Hampton, Va., December 6, 1973.

APPENDIX

ANALYSIS

This appendix develops the expression which relates the change in rolling radius of tires under steady-state braking conditions to previously defined tire elastic properties.

The experimental data presented herein indicate that the tread deformation in the leading half of the footprint can be expressed by the following equation:

$$u_f = u_{f0} + ms_f \tag{A1}$$

The maximum deformation within the footprint is by definition

$$u_{f0} = \frac{F_x}{K_x} \tag{A2}$$

Substituting equation (A2) into equation (A1) and normalizing yield

$$\frac{K_x}{F_x} u_f = 1 + Ms_f \tag{A3}$$

where

$$M = \frac{m}{u_{f0}} \tag{A4}$$

The elongation strain in the footprint due to the braking effort is defined as

$$\epsilon_{x,f} = \frac{du_f}{ds_f} = \frac{F_x}{K_x} M \tag{A5}$$

The tread stretch which has accumulated within the footprint can be determined by integrating equation (A5) over the half-length of the footprint to yield

$$Q_f = \int_0^h du_f = - \frac{F_x}{K_x} Mh \tag{A6}$$

The static data presented herein indicated that the tread deformation along the free periphery near the footprint leading edge can be expressed as

$$u_p = \frac{F_x}{K_x} e^{-s_p/J_x} \qquad \left(0 \leqq s_p \leqq s_{p,max}\right) \tag{A7}$$

and the maximum deformation was assumed to occur at the footprint leading edge. Under rolling conditions, however, equation (A7) must be modified to conform to the following boundary condition:

$$u_f\big|_{s_f=h} = u_p\big|_{s_p=0} \tag{A8}$$

where

$$u_f\big|_{s_f=h} = \frac{F_x}{K_x} + mh \tag{A9}$$

Equation (A7) now becomes

$$u_p = \frac{F_x}{K_x}(1 + Mh)e^{-s_p/J_x} \qquad \left(0 \leqq s_p \leqq s_{p,max}\right) \tag{A10}$$

The elongation strain in the free periphery due to the braking effort is defined by

$$\epsilon_{x,p} = \frac{du_p}{ds_p} = -\frac{F_x}{J_x K_x}(1 + Mh)e^{-s_p/J_x} \tag{A11}$$

The tread stretch which has accumulated in the free periphery can be determined by integrating equation (A11) over the appropriate limits of integration

$$Q_p = \int du_p = \frac{F_x}{K_x}(1 + Mh)\int_{s_{p,max}}^{0} -\frac{1}{J_x} e^{-s_p/J_x}\, ds_p \tag{A12}$$

Performing the indicated integration yields

$$Q_p = \frac{F_x}{K_x}(1 + Mh)e^{-s_p/J_x}\Big|_{s_{p,max}}^{0} \tag{A13}$$

or

$$Q_p = \frac{F_x}{K_x}(1 + Mh)\left(1 - e^{-s_{p,max}/J_x}\right) \tag{A14}$$

The total tread stretch due to the braking effort is

$$Q_t = Q_f + Q_p \tag{A15}$$

Equation (A15) represents the net increase in tire circumference due to braking forces, and the net change in rolling radius is obtained by dividing equation (A15) by 2π to yield

$$\Delta R = \frac{Q_t}{2\pi} = \frac{F_x}{2\pi K_x}\left[1 - (1 + Mh)e^{-s_{p,max}/J_x}\right]$$

This equation is a general expression which may be used to compute the change in rolling radius due to the braking effort regardless of the tire construction.

REFERENCES

1. Davis, J. E.; and Curry, R. C.: The Costs of Landing an Airplane. SAE J., vol. 71, Dec. 1963, pp. 47-49.

2. Batterson, Sidney A.: A Study of the Dynamics of Airplane Braking Systems as Affected by Tire Elasticity and Brake Response. NASA TN D-3081, 1965.

3. Tanner, John A.: Performance of an Aircraft Tire Under Cyclic Braking and of a Currently Operational Antiskid Braking System. NASA TN D-6755, 1972.

4. Bourcier de Carbon, Christian: Étude Théorique du Shimmy des Roues d'Avion (Analytical Study of Shimmy of Airplane Wheels). O.N.E.R.A. Publ. No. 7, 1948. (Available in English translation as NACA TM 1337.)

5. Förster, B.: Versuche zur Feststellung des Haftvermögens von Personenwagen-Bereifungen (Tests To Determine the Adhesive Power of Passenger-Car Tires). Deutsche Kraftfahrtforschung ZB Nr. 22. (Available in English translation as NACA TM 1416.)

6. Fromm, H.: Seitenschlupf und Führungswert des rollenden Rades (Sideslip and Guiding Characteristics of the Rolling Wheel). Bericht 140 der L.G.L., 1941, pp. 56-63. (Available in English translation as NACA TM 1365, pp. 191-216.)

7. Fromm, H.: Schwingungsdämpfung am rollenden Rade (Oscillation Damping on the Rolling Wheel). Bericht 140 der L.G.L., 1941, pp. 66-67. (Available in English translation as NACA TM 1365, pp. 229-233.)

8. Horne, Walter B.: Static Force-Deflection Characteristics of Six Aircraft Tires Under Combined Loading. NACA TN 2926, 1953.

9. Horne, Walter B.; Stephenson, Bertrand H.; and Smiley, Robert F.: Low-Speed Yawed-Rolling and Some Other Elastic Characteristics of Two 56-Inch-Diameter, 24-Ply-Rating Aircraft Tires. NACA TN 3235, 1954.

10. Horne, Walter B.; and Smiley, Robert F.: Low-Speed Yawed-Rolling Characteristics and Other Elastic Properties of a Pair of 40-Inch-Diameter, 14-Ply-Rating, Type VII Aircraft Tires. NACA TN 4109, 1958.

11. Kantrowitz, Arthur: Stability of Castering Wheels for Aircraft Landing Gears. NACA Rep. 686, 1940.

12. Boeckh: Ermittlung der elastischen Konstanten von Flugzeugreifen (Determination of the Elastic Constants of Airplane Tires). Focke-Wulf Flugzeugbau G.m.b.H. (Bremen), Dec. 1944. (Available in English translation as NACA TM 1378.)

13. Smiley, Robert F.; and Horne, Walter B.: Mechanical Properties of Pneumatic Tires With Special Reference to Modern Aircraft Tires. NASA TR R-64, 1960. (Supersedes NACA TN 4110.)

14. Tanner, John A.; McCarty, John L.; and Batterson, Sidney A.: The Elastic Response of Bias-Ply Aircraft Tires to Braking Forces. NASA TN D-6426, 1971.

15. Anon.: Metric Practice Guide. E 380-72, Amer. Soc. Testing Mater., June 1972.

16. Hoel, Paul G.: Introduction to Mathematical Statistics. Third ed., John Wiley & Sons, Inc., c.1962.

17. Draper, N. R.; and Smith, H.: Applied Regression Analysis. John Wiley & Sons, Inc., c.1966.

18. Hicks, Charles R.: Fundamental Concepts in the Design of Experiments. Holt, Rinehart and Winston, Inc., c.1964.

TABLE I.- TIRE SPECIFICATIONS

Item	Bias ply	Bias belted	Radial belted
Bead	Wire, steel	Wire, steel	Wire, steel
Carcass: Matrix Cord	 Natural rubber Nylon	 Natural rubber Nylon	 Natural rubber Nylon
Belt	None	Polyester	Steel
Tread: Material Groove pattern	 Natural rubber 5-groove	 Natural rubber 4-groove	 Natural rubber 4-groove
Rated inflation pressure	793 kPa (115 lb/in^2)	793 kPa (115 lb/in^2)	793 kPa (115 lb/in^2)
Rated vertical load	58.7 kN (13 200 lb)	58.7 kN (13 200 lb)	58.7 kN (13 200 lb)
Unloaded circumference	[a]264.9 cm (104.3 in.) [c]265.7 cm (104.6 in.) [d]266.4 cm (104.9 in.)	[b]268.2 cm (105.6 in.)	[b]263.4 cm (103.7 in.)

[a]Inflation pressure of 621 kPa (90 lb/in^2).

[b]All test inflation pressures.

[c]Inflation pressure of 793 kPa (115 lb/in^2).

[d]Inflation pressure of 965 kPa (140 lb/in^2).

TABLE II.- SUMMARY OF FORE-AND-AFT SPRING CONSTANTS FROM STATIC TEST

p		F_z		Bias ply				Bias belted				Radial belted			
				K_x		δ		K_x		δ		K_x		δ	
kPa	lb/in^2	kN	lb	kN/m	lb/in.	cm	in.	kN/m	lb/in.	cm	in.	kN/m	lb/in.	cm	in.
621	90	51.2	11 500	899	5133	6.83	2.69	1000	5709	7.14	2.81	746	4260	8.10	3.19
		58.7	13 200	918	5240	7.47	2.94	968	5525	8.26	3.25	743	4240	9.04	3.56
		66.8	15 000	915	5226	8.89	3.50	987	5634	8.74	3.44	679	3879	10.16	4.00
793	115	51.2	11 500	1081	6173	5.56	2.19	1182	6749	6.20	2.44	825	4710	6.83	2.69
		58.7	13 200	1103	6296	6.20	2.44	1156	6601	6.83	2.69	862	4920	7.62	3.00
		66.8	15 000	1084	6191	6.83	2.69	1150	6565	7.14	2.81	708	4045	8.10	3.19
965	140	51.2	11 500	1173	6696	4.93	1.94	1359	7762	5.08	2.00	895	5110	6.35	2.50
		58.7	13 200	1235	7051	5.38	2.12	1317	7519	5.87	2.31	953	5440	6.83	2.69
		66.8	15 000	1213	6928	5.72	2.25	1206	6889	6.35	2.50	844	4820	7.32	2.88

TABLE III.- SUMMARY OF FORE-AND-AFT DECAY LENGTHS FROM STATIC TESTS

(a) Bias-ply tire; $s_{p,max}$ = 35.6 cm (14 in.)

p		F_z		F_x		J_x		r
kPa	lb/in^2	kN	lb	kN	lb	cm	in.	
621	90	51.2	11 500	8.9	2000	62.0	24.4	-0.926
				13.4	3000	40.6	16.0	-.971
				17.8	4000	43.2	17.0	-.961
		58.7	13 200	8.9	2000	186.9	73.6	-0.633
				13.4	3000	51.6	20.3	-.944
				17.8	4000	58.7	23.1	-.953
		66.8	15 000	8.9	2000	91.4	36.0	-0.903
				13.4	3000	43.4	17.1	-.972
				17.8	4000	51.0	20.1	-.967
793	115	51.2	11 500	8.9	2000	53.8	21.2	-0.935
				13.4	3000	43.9	17.3	-.956
				17.8	4000	55.6	21.9	-.915
		58.7	13 200	8.9	2000	83.8	33.0	-0.876
				13.4	3000	46.2	18.2	-.959
				17.8	4000	51.8	20.4	-.944
		66.8	15 000	8.9	2000	97.0	38.2	-0.817
				13.4	3000	52.3	20.6	-.967
				17.8	4000	63.8	25.1	-.924
965	140	51.2	11 500	8.9	2000	124.2	48.9	-0.844
				13.4	3000	73.2	28.8	-.920
				17.8	4000	88.1	34.7	-.893
		58.7	13 200	8.9	2000	88.1	34.7	-0.804
				13.4	3000	72.9	28.7	-.905
				17.8	4000	65.0	25.6	-.915
		66.8	15 000	8.9	2000	117.6	46.3	-0.852
				13.4	3000	67.0	26.4	-.967
				17.8	4000	89.4	35.2	-.929

TABLE III.- SUMMARY OF FORE-AND-AFT DECAY LENGTHS FROM STATIC TESTS – Continued

(b) Bias-belted tire; $s_{p,max}$ = 35.6 cm (14 in.)

p		F_z		F_x		J_x		r
kPa	lb/in^2	kN	lb	kN	lb	cm	in.	
621	90	51.2	11 500	8.9	2000	(a)	(a)	(a)
				13.4	3000	59.2	23.3	-0.962
				17.8	4000	66.0	26.0	-.949
		58.7	13 200	8.9	2000	71.9	28.3	-0.978
				13.4	3000	61.7	24.3	-.967
				17.8	4000	54.6	21.5	-.975
		66.8	15 000	8.9	2000	82.3	32.4	-0.964
				13.4	3000	65.0	25.6	-.978
				17.8	4000	(a)	(a)	(a)
793	115	51.2	11 500	8.9	2000	45.7	18.0	-0.972
				13.4	3000	56.6	22.3	-.960
				17.8	4000	55.1	21.7	-.984
		58.7	13 200	8.9	2000	(a)	(a)	(a)
				13.4	3000	53.1	20.9	-0.968
				17.8	4000	(a)	(a)	(a)
		66.8	15 000	8.9	2000	240.8	94.8	-0.659
				13.4	3000	112.5	44.3	-.933
				17.8	4000	103.9	40.9	-.940
965	140	51.2	11 500	8.9	2000	64.3	25.3	-0.825
				13.4	3000	41.9	16.5	-.961
				17.8	4000	46.2	18.2	-.946
		58.7	13 200	8.9	2000	75.2	29.6	-0.959
				13.4	3000	55.4	21.8	-.975
				17.8	4000	48.3	19.0	-.978
		66.8	15 000	8.9	2000	82.6	32.5	-0.980
				13.4	3000	83.3	32.8	-.975
				17.8	4000	78.5	30.9	-.967

[a]Data not available.

TABLE III.- SUMMARY OF FORE-AND-AFT DECAY LENGTHS FROM STATIC TESTS – Concluded

(c) Radial-belted tire; $s_{p,max}$ = 35.6 cm (14 in.)

p		F_z		F_x		J_x		r
kPa	lb/in^2	kN	lb	kN	lb	cm	in.	(a)
621	90	51.2	11 500	8.9	2000	∞	∞	N.A.
				13.4	3000	∞	∞	N.A.
				17.8	4000	∞	∞	N.A.
		58.7	13 200	8.9	2000	∞	∞	N.A.
				13.4	3000	∞	∞	N.A.
				17.8	4000	∞	∞	N.A.
		66.8	15 000	8.9	2000	∞	∞	N.A.
				13.4	3000	∞	∞	N.A.
				17.8	4000	∞	∞	N.A.
793	115	51.2	11 500	8.9	2000	∞	∞	N.A.
				13.4	3000	∞	∞	N.A.
				17.8	4000	∞	∞	N.A.
		58.7	13 200	8.9	2000	∞	∞	N.A.
				13.4	3000	∞	∞	N.A.
				17.8	4000	∞	∞	N.A.
		66.8	15 000	8.9	2000	∞	∞	N.A.
				13.4	3000	∞	∞	N.A.
				17.8	4000	∞	∞	N.A.
965	140	51.2	11 500	8.9	2000	∞	∞	N.A.
				13.4	3000	∞	∞	N.A.
				17.8	4000	∞	∞	N.A.
		58.7	13 200	8.9	2000	∞	∞	N.A.
				13.4	3000	∞	∞	N.A
				17.8	4000	∞	∞	N.A.
		66.8	15 000	8.9	2000	∞	∞	N.A.
				13.4	3000	∞	∞	N.A.
				17.8	4000	∞	∞	N.A.

[a]N.A. denotes data not applicable.

TABLE IV.- SUMMARY OF TREAD DEFORMATION VARIATION WITHIN BRAKED-ROLLING FOOTPRINT

(a) Bias-ply tire

p		F_Z		h		F_X		M		r
kPa	lb/in^2	kN	lb	cm	in.	kN	lb	m^{-1}	in^{-1}	
621	90	51.2	11 500	18.80	7.40	9.0	2031	-2.362	-0.060	-0.990
						17.6	3960	-2.756	-.070	-.998
						20.2	4529	-3.386	-.086	-.994
		58.7	13 200	19.51	7.68	10.5	2364	-1.496	-0.038	-0.991
						15.9	3567	-2.953	-.075	-.999
						21.8	4890	-3.346	-.085	-.998
		66.8	15 000	20.29	7.99	10.2	2291	-1.929	-0.049	-0.974
						15.6	3500	-2.913	-.074	-.990
						22.3	5004	-2.913	-.074	-.999
793	115	51.2	11 500	17.53	6.90	9.5	2131	-1.969	-0.050	-0.980
						16.6	3725	-4.055	-.103	-.999
						22.5	5050	-4.685	-.119	-.995
		58.7	13 200	18.97	7.47	9.5	2131	-2.126	-0.054	-0.969
						16.8	3783	-3.425	-.087	-.998
						21.0	4731	-4.016	-.102	-.999
		66.8	15 000	18.82	7.41	10.2	2302	-2.165	-0.055	-0.993
						16.4	3698	-3.425	-.087	-.998
						21.9	4924	-3.307	-.084	-.999
965	140	51.2	11 500	16.13	6.35	8.8	1984	-2.992	-0.076	-0.995
		51.2	11 500	16.13	6.35	15.2	3422	-4.449	-.113	-.999
		58.7	13 200	17.40	6.85	8.1	1814	-3.268	-0.083	-0.986
						15.7	3526	-4.291	-.109	-.995
						20.6	4638	-4.882	-.124	-.997
		66.8	15 000	17.73	6.98	8.3	1865	-2.244	-0.057	-0.984
						17.2	3854	-3.701	-.094	-.999
						23.0	5181	-3.740	-.095	-1.000

TABLE IV.- SUMMARY OF TREAD DEFORMATION VARIATION WITHIN BRAKED-ROLLING FOOTPRINT – Continued

(b) Bias-belted tire

p		F_z		h		F_x		M		r
kPa	lb/in^2	kN	lb	cm	in.	kN	lb	m^{-1}	in^{-1}	
621	90	51.2	11 500	19.43	7.65	15.8	3548	-2.087	-0.053	-0.992
		51.2	11 500	19.43	7.65	19.1	4289	-2.559	-.065	-.994
		58.7	13 200	20.07	7.90	8.6	1931	-2.795	-0.071	-0.957
						10.4	2338	-2.835	-.072	-.986
						13.5	3039	-2.795	-.071	-.990
		66.8	15 000	20.88	8.22	9.2	2065	-2.480	-0.063	-0.988
						12.5	2806	-2.598	-.066	-.995
						19.7	4437	-2.559	-.065	-.994
793	115	51.2	11 500	17.78	7.00	8.9	1992	-2.559	-0.065	-0.950
						11.6	2608	-3.268	-.083	-.991
						17.3	3882	-3.976	-.101	-.997
		58.7	13 200	19.43	7.65	8.9	1998	-3.740	-0.095	-0.994
						10.6	2383	-2.835	-.072	-.982
						12.8	2876	-3.228	-.082	-.998
		66.8	15 000	19.43	7.65	9.5	2137	-1.575	-0.040	-0.957
						13.4	3024	-2.402	-.061	-.997
						18.8	4231	-2.874	-.073	-.995
965	140	51.2	11 500	17.35	6.83	8.0	1803	-3.189	-0.081	-0.962
						15.5	3490	-3.898	-.099	-.991
						18.6	4173	-3.465	-.088	-.996
		58.7	13 200	18.14	7.14	7.2	1611	-2.323	-0.059	-0.883
						8.4	1881	-2.559	-.065	-.982
						10.3	2308	-2.835	-.072	-.972
		66.8	15 200	18.14	7.14	8.9	1992	-2.283	-0.058	-0.952
						13.1	2951	-3.268	-.083	-.995
						18.8	4231	-3.150	-.080	-.993

TABLE IV.- SUMMARY OF TREAD DEFORMATION VARIATION WITHIN BRAKED-ROLLING FOOTPRINT – Concluded

(c) Radial-belted tire

p		F_z		h		F_x		M		r
kPa	lb/in^2	kN	lb	cm	in.	kN	lb	m^{-1}	in^{-1}	(a)
621	90	51.2	11 500	19.84	7.81	11.0	2468	0	0	N.A.
						14.9	3353	0	0	N.A.
						18.5	4151	0	0	N.A.
		58.7	13 200	19.86	7.82	7.8	1743	0	0	N.A.
						11.3	2541	0	0	N.A.
						16.9	3803	0	0	N.A.
		66.8	15 000	20.02	7.88	8.0	1800	0	0	N.A.
						11.1	2500	0	0	N.A.
						19.1	4300	0	0	N.A.
793	115	51.2	11 500	18.95	7.46	8.3	1858	0	0	N.A.
						14.5	3250	0	0	N.A.
						20.7	4649	0	0	N.A.
		58.7	13 200	18.97	7.47	9.2	2062	0	0	N.A.
						11.9	2671	0	0	N.A.
						19.8	4442	0	0	N.A.
		66.8	15 000	19.00	7.48	8.9	2000	0	0	N.A.
						11.1	2500	0	0	N.A.
						20.0	4500	0	0	N.A.
965	140	51.2	11 500	18.67	7.35	10.2	2300	0	0	N.A.
						15.2	3425	0	0	N.A.
						17.8	4000	0	0	N.A.
		58.7	13 200	18.69	7.36	8.9	2000	(b)	(b)	(b)
						13.4	3000	(b)	(b)	(b)
						17.8	4000	(b)	(b)	(b)
		66.2	15 000	18.74	7.38	8.9	2000	(b)	(b)	(b)
						13.6	3000	(b)	(b)	(b)
						17.8	4000	(b)	(b)	(b)

[a]N.A. denotes data not applicable.

[b]Data not available.

TABLE V.- SUMMARY OF ROLLING RADIUS DATA

(a) Bias-ply tire

Speed, knots	p		F_z		F_x		ΔR_{calc} (a)		ΔR_{exp}	
	kPa	lb/in^2	kN	lb	kN	lb	cm	in.	cm	in.
5	965	140	56.3	12 664	19.2	4324	0.18	0.07	2.34	0.92
5	965	140	62.3	14 007	18.5	4165	.18	.07	1.68	.66
5	793	115	56.8	12 761	20.2	4531	.20	.08	2.39	.94
5	793	115	64.5	14 486	19.0	4268	.18	.07	2.16	.85
5	621	90	55.5	12 477	16.8	3788	.15	.06	1.96	.77
5	621	90	64.5	14 492	15.7	3526	.13	.05	1.42	.56
5	965	140	70.9	15 926	14.5	3254	.10	.04	1.73	.68
5	793	115	72.6	16 311	15.7	3528	.10	.04	1.73	.68
5	621	90	70.9	15 926	15.7	3528	.10	.04	1.73	.68
98.0	965	140	58.6	13 161	8.7	1957	.05	.02	.71	.28
98.0	965	140	57.6	12 950	15.2	3425	.13	.05	1.50	.59
97.3	965	140	57.9	13 022	20.5	4606	.23	.09	2.13	.84
100.0	965	140	66.9	15 035	19.2	4326	.18	.07	1.88	.74
103.0	965	140	65.7	14 773	14.4	3238	.10	.04	1.37	.54
104.0	965	140	65.7	14 768	9.4	2110	.05	.02	.74	.29
103.0	965	140	72.7	16 333	8.8	1985	.05	.02	.66	.26
99.0	965	140	72.6	16 308	15.1	3400	.10	.04	1.32	.52
98.0	965	140	73.6	16 543	20.6	4624	.18	.07	1.91	.75
99.0	793	115	58.7	13 196	13.4	3023	.10	.04	2.08	.82
99.0	793	115	58.4	13 119	14.1	3167	.13	.05	1.47	.58
103.0	793	115	57.8	12 998	8.3	1873	.05	.02	.71	.28
100.0	793	115	57.3	12 879	8.8	1973	.05	.02	.74	.29
104.0	793	115	65.4	14 710	15.8	3545	.13	.05	1.35	.53
101.0	793	115	69.3	15 583	20.9	4689	.20	.08	1.96	.77
101.0	793	115	74.0	16 618	19.4	4367	.15	.06	1.65	.65
102.0	793	115	73.0	16 404	15.1	3404	.10	.04	1.22	.48
103.0	793	115	71.4	16 046	10.2	2295	.05	.02	.64	.25
107.0	621	90	56.8	12 757	8.9	2010	.05	.02	.51	.20
107.0	621	90	56.8	12 753	15.6	3515	.13	.05	1.55	.61
107.0	621	90	57.2	12 851	17.1	3841	.15	.06	1.98	.78
99.0	621	90	66.0	14 821	18.6	4172	.15	.06	1.63	.64
99.5	621	90	64.2	14 439	15.0	3370	.10	.04	1.32	.52
97.0	621	90	66.3	14 893	20.7	4658	.20	.08	1.73	.68
100.0	621	90	72.2	16 225	20.4	4579	.18	.07	1.42	.56
101.0	621	90	71.9	16 156	14.7	3304	.08	.03	.91	.36
100.0	621	90	72.9	16 376	9.4	2118	.02	.01	.46	.18

[a]From equation (14).

TABLE V.- SUMMARY OF ROLLING RADIUS DATA – Continued

(b) Bias-belted tire

Speed, knots	p		F_z		F_x		ΔR_{calc} (a)		ΔR_{exp}	
	kPa	lb/in^2	kN	lb	kN	lb	cm	in.	cm	in.
5	965	140	68.8	15 472	13.7	3084	0.08	0.03	1.17	0.46
5	793	115	70.9	15 936	14.4	3229	.10	.04	(b)	(b)
5	621	90	69.6	15 648	16.5	3710	.13	.05	1.45	.57
5	965	140	56.0	12 578	6.9	1556	.05	.02	.41	.16
5	965	140	64.1	14 404	14.6	3288	.10	.04	1.47	.58
5	793	115	55.6	12 484	15.0	3374	.10	.04	1.55	.61
5	793	115	63.2	14 213	15.3	3433	.13	.05	1.40	.55
5	621	90	54.7	12 293	15.5	3491	.13	.05	1.30	.51
98.7	965	140	58.8	13 204	14.6	3289	.10	.04	.94	.37
100.4	965	140	61.3	13 767	11.3	2543	.08	.03	.79	.31
101.6	965	140	65.6	14 732	11.1	2500	.08	.03	.79	.31
102.3	965	140	63.3	14 231	8.5	1914	.05	.02	.91	.36
97.5	965	140	57.1	12 826	8.5	1902	.05	.02	.56	.22
98.7	793	115	66.5	14 952	8.3	1857	.05	.02	.89	.35
98.7	621	90	58.3	13 101	11.3	2543	.10	.04	.86	.34
100.6	793	115	72.3	16 249	9.6	2167	.05	.02	.46	.18
98.8	793	115	72.9	16 379	12.0	2699	.08	.03	.33	.13
99.7	793	115	73.1	16 430	16.3	3660	.10	.04	1.02	.40
97.2	793	115	67.0	15 064	11.7	2638	.08	.03	.74	.29
98.5	793	115	67.4	15 154	16.1	3626	.13	.05	.86	.34
103.0	965	140	73.9	16 615	8.6	1924	.05	.02	.41	.16
98.9	965	140	71.4	16 049	12.3	2773	.08	.03	.74	.29
100.2	965	140	73.6	16 550	14.7	3305	.08	.03	.94	.37
94.3	965	140	68.1	15 311	15.2	3424	.10	.04	1.63	.64
97.2	793	115	58.5	13 145	8.5	1918	.05	.02	.48	.19
97.2	793	115	59.8	13 430	11.2	2509	.08	.03	.71	.28
97.2	793	115	60.6	13 623	14.7	3295	.10	.04	.94	.37
101.0	621	90	59.2	13 297	14.0	3149	.10	.04	.79	.31
101.0	621	90	67.0	15 064	8.5	1915	.05	.02	.41	.16
97.5	621	90	65.5	14 719	11.3	2535	.08	.03	.68	.27
97.5	621	90	67.2	15 109	14.4	3248	.13	.05	1.02	.40
98.8	621	90	74.7	16 789	8.8	1974	.05	.02	.38	.15
96.0	621	90	73.0	16 404	11.9	2669	.08	.03	.53	.21
99.7	621	90	74.3	16 692	15.4	3459	.13	.05	.91	.36
100.6	793	115	67.4	15 158	16.8	3773	.13	.05	1.12	.44
89.0	793	115	58.9	13 239	19.8	4455	.15	.06	1.02	.40
101.0	793	115	59.3	13 333	18.8	4216	.15	.06	1.80	.71
93.5	793	115	58.9	13 239	18.8	4216	.15	.06	1.40	.55
98.7	621	90	58.3	13 105	8.9	2009	.08	.03	.28	.11

[a]From equation (14).

[b]Data not available.

TABLE V.- SUMMARY OF ROLLING RADIUS DATA – Concluded

(c) Radial-belted tire

Speed, knots	p		F_z		F_x		ΔR_{calc} (a)		ΔR_{exp}	
	kPa	lb/in^2	kN	lb	kN	lb	cm	in.	cm	in.
5	965	140	51.2	11 500	9.6	2150	0	0	0.48	0.19
5	965	140	58.7	13 200	11.3	2550	0	0	.46	.18
5	965	140	66.8	15 000	13.5	3025	0	0	.25	.10
5	793	115	51.2	11 500	11.1	2500	0	0	.36	.14
5	793	115	58.7	13 200	11.8	2650	0	0	.20	.08
5	793	115	66.8	15 000	14.0	3150	0	0	.25	.10
5	621	90	51.2	11 500	12.0	2700	0	0	.25	.10
5	621	90	58.7	13 200	14.7	3300	0	0	.20	.08
5	621	90	66.8	15 000	16.1	3625	0	0	.20	.08
97.1	965	140	66.5	14 952	8.5	1902	0	0	.20	.08
101.0	965	140	58.1	13 047	5.7	1277	0	0	.13	.05
100.2	965	140	59.2	13 293	11.8	2646	0	0	.36	.14
101.1	793	115	66.4	14 924	7.4	1663	0	0	.10	.04
101.5	793	115	67.0	15 061	10.7	2404	0	0	.13	.05
100.6	793	115	65.0	14 620	13.4	3022	0	0	.15	.06
99.2	965	140	66.2	14 867	7.0	1586	0	0	.20	.08
98.3	965	140	66.6	14 964	10.9	2448	0	0	.33	.13
97.7	965	140	67.4	15 139	14.4	3248	0	0	.41	.16
101.1	793	115	58.9	13 239	8.0	1802	0	0	.13	.05

[a]From equation (14).

Bias ply

Bias belted

Radial belted

L-73-8038

Figure 1.- Aircraft tires used in the investigation.

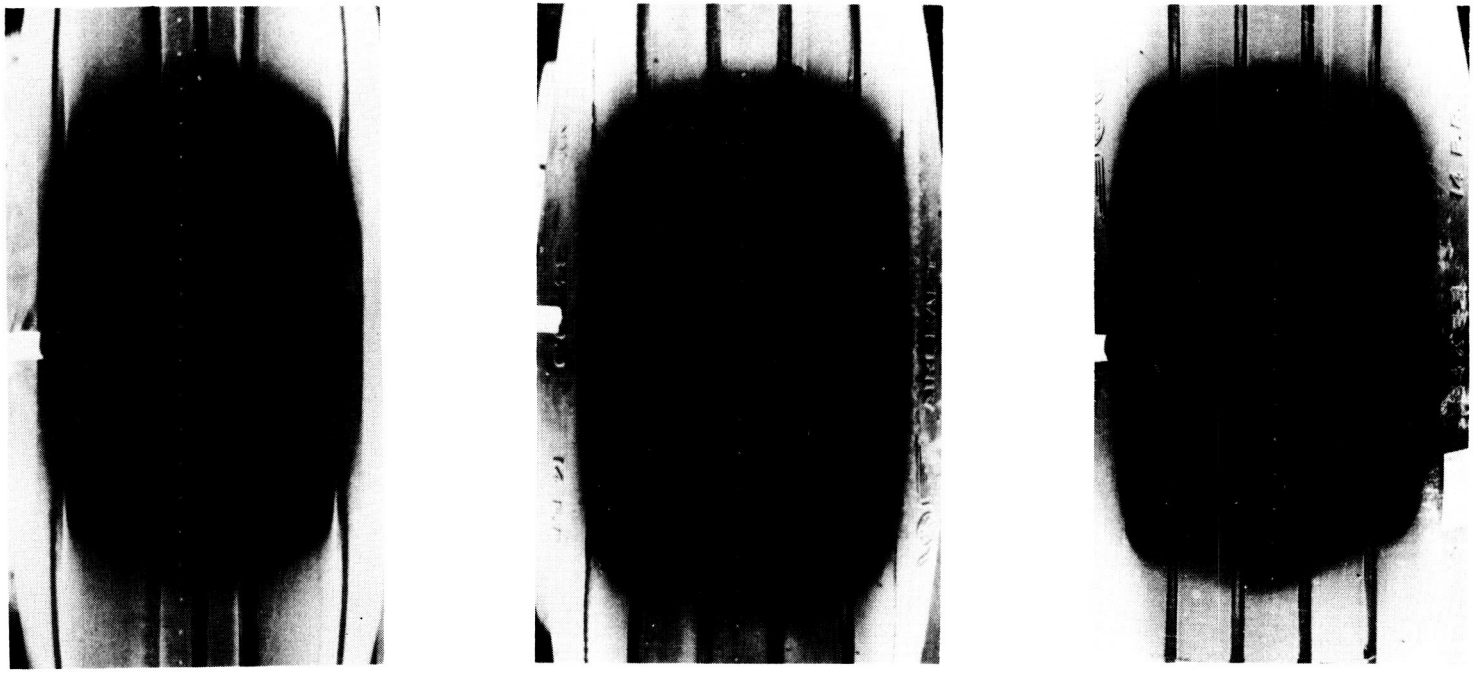

Bias ply | Bias belted | Radial belted

L-73-8039

Figure 2.- Tire footprints as seen from beneath glass plate.

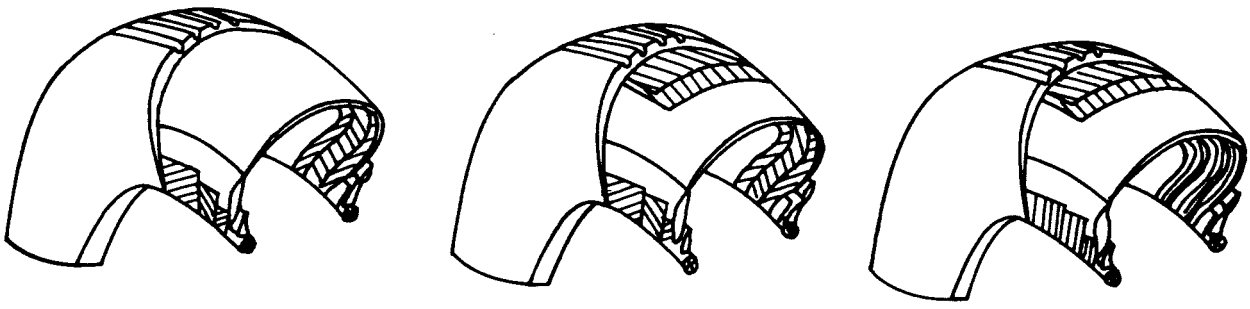

Figure 3.-Sketches illustrating the different tire constructions.

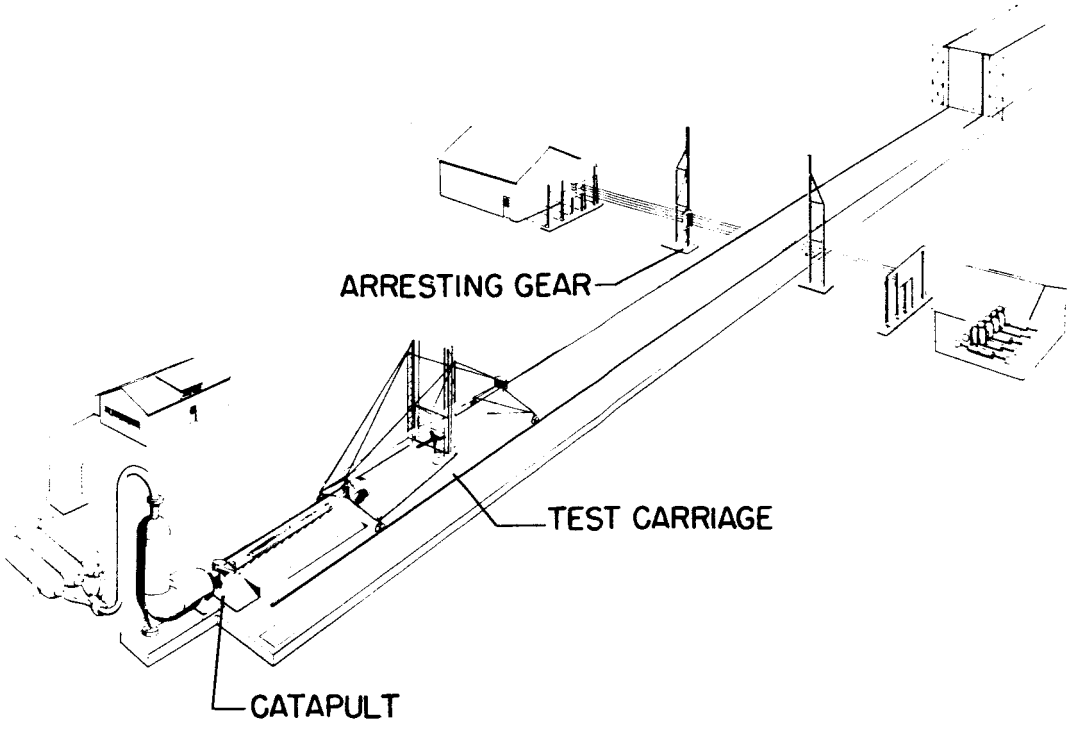

Figure 4.- Schematic of aircraft landing loads and traction facility.

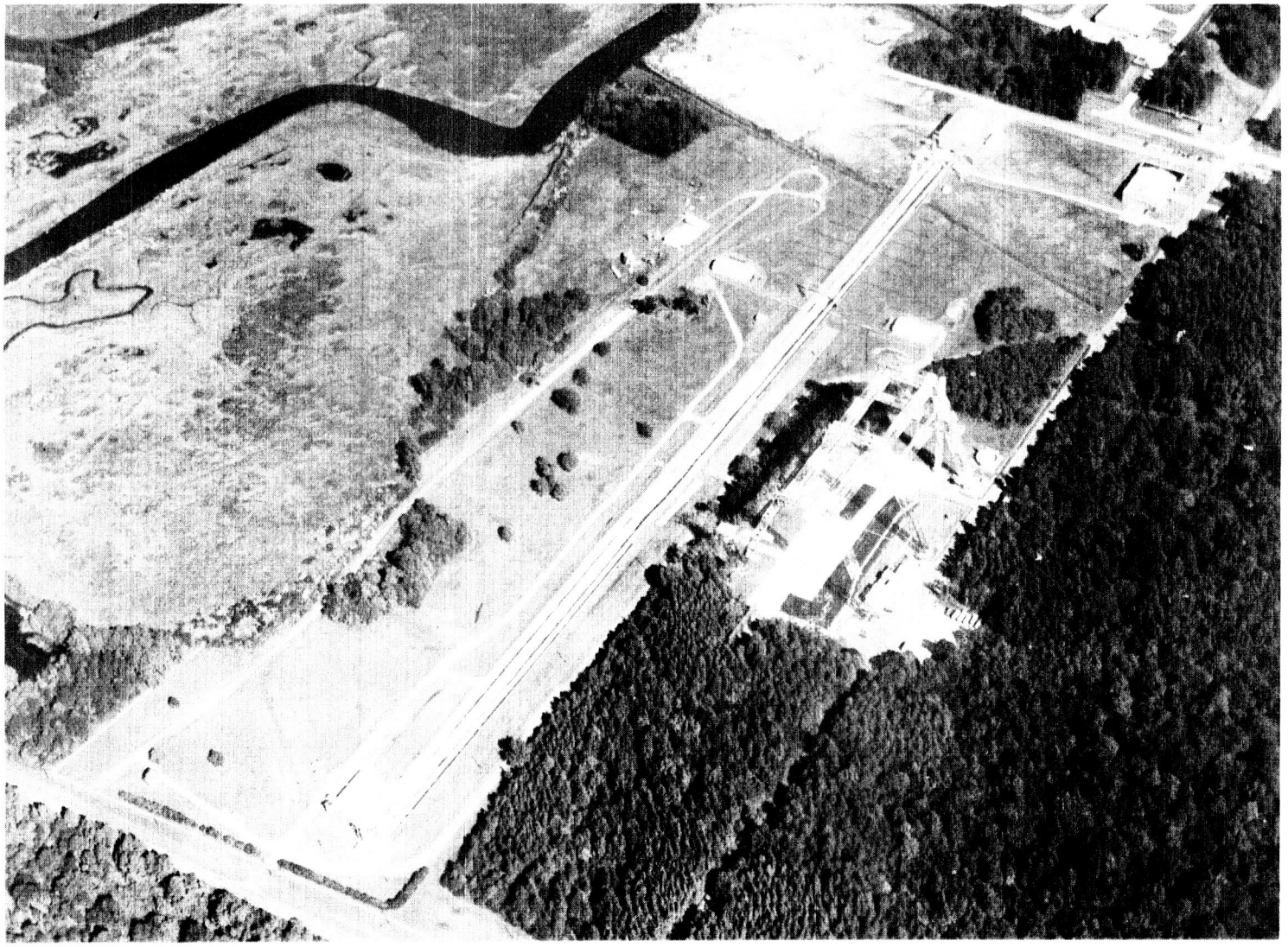

L-73-8040

Figure 5.- Aerial photograph of test facility.

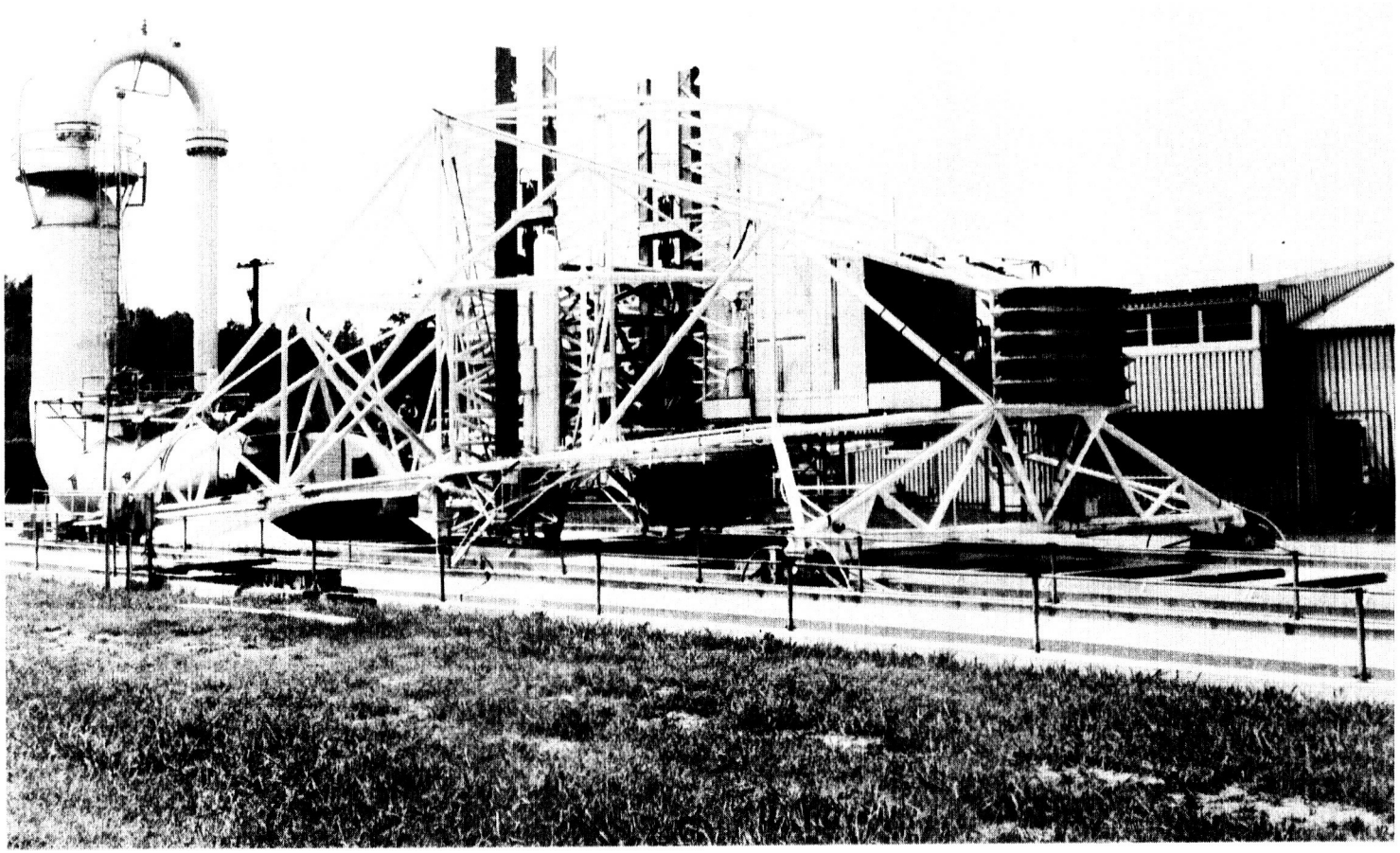

L-69-5860

Figure 6.- Test carriage and L-shaped pressure vessel.

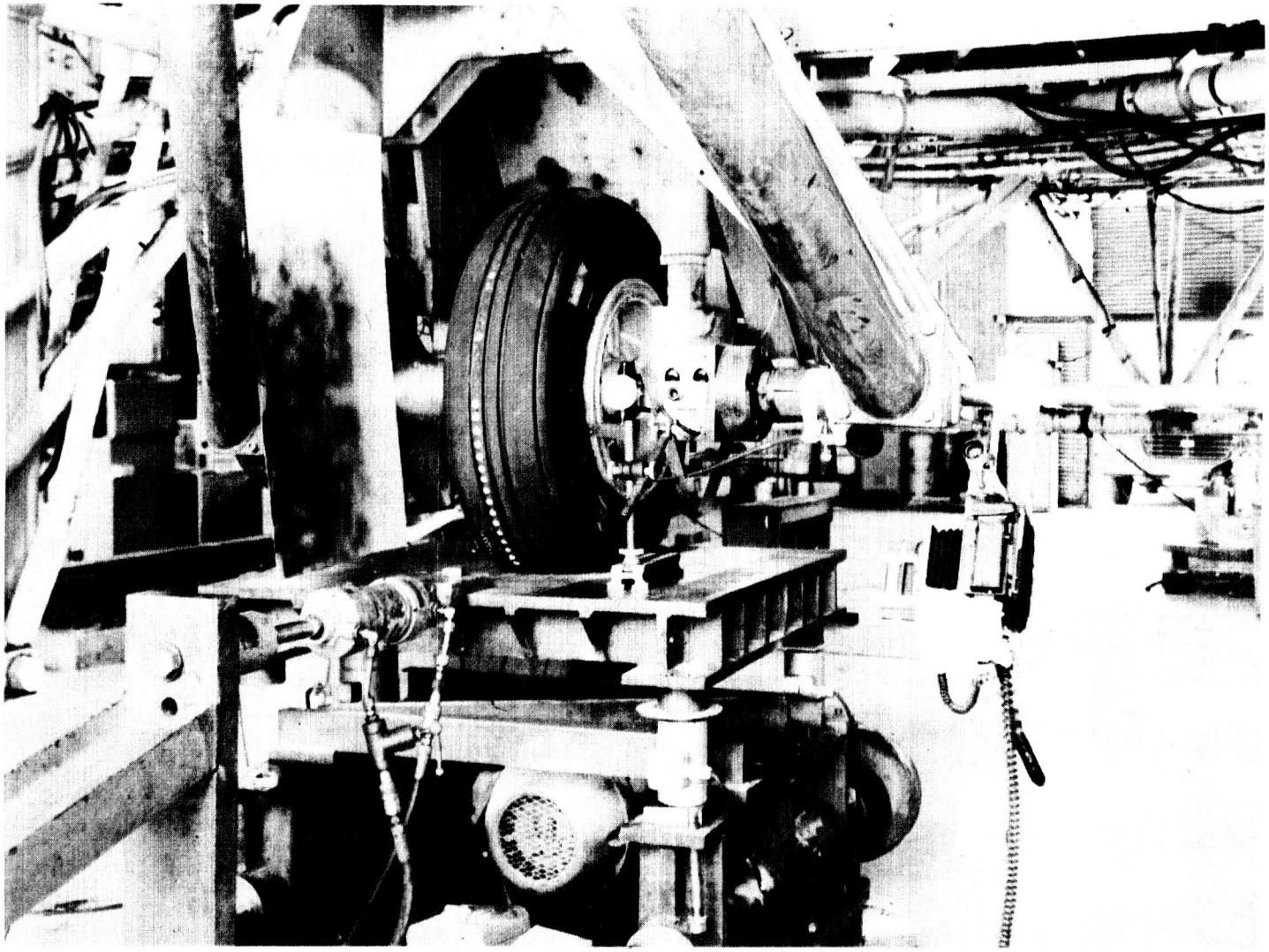

L-73-8041

Figure 7.- Static test equipment.

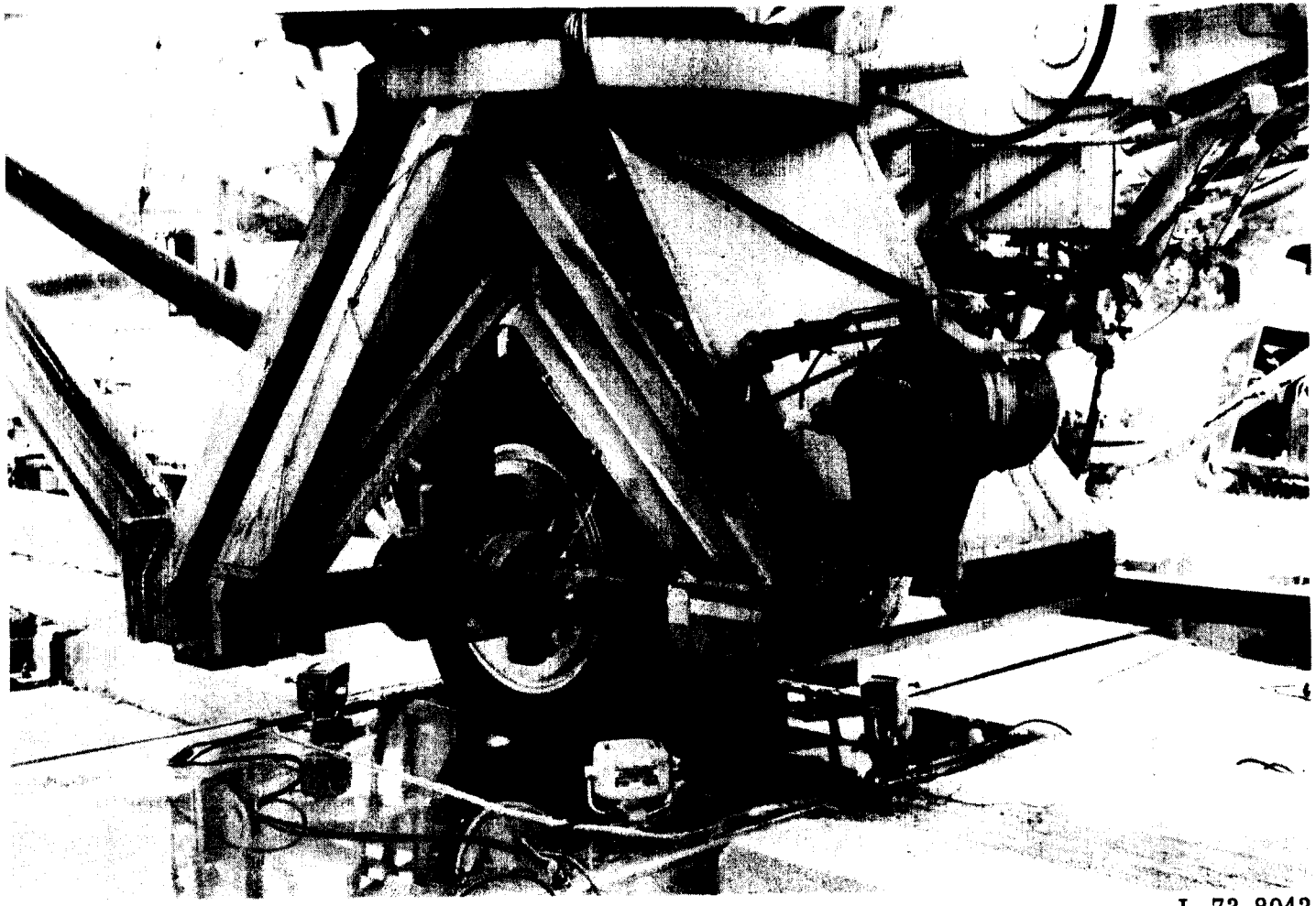

L-73-8042

Figure 8.- Tire and instrumented dynamometer during braked-rolling test over glass plate.

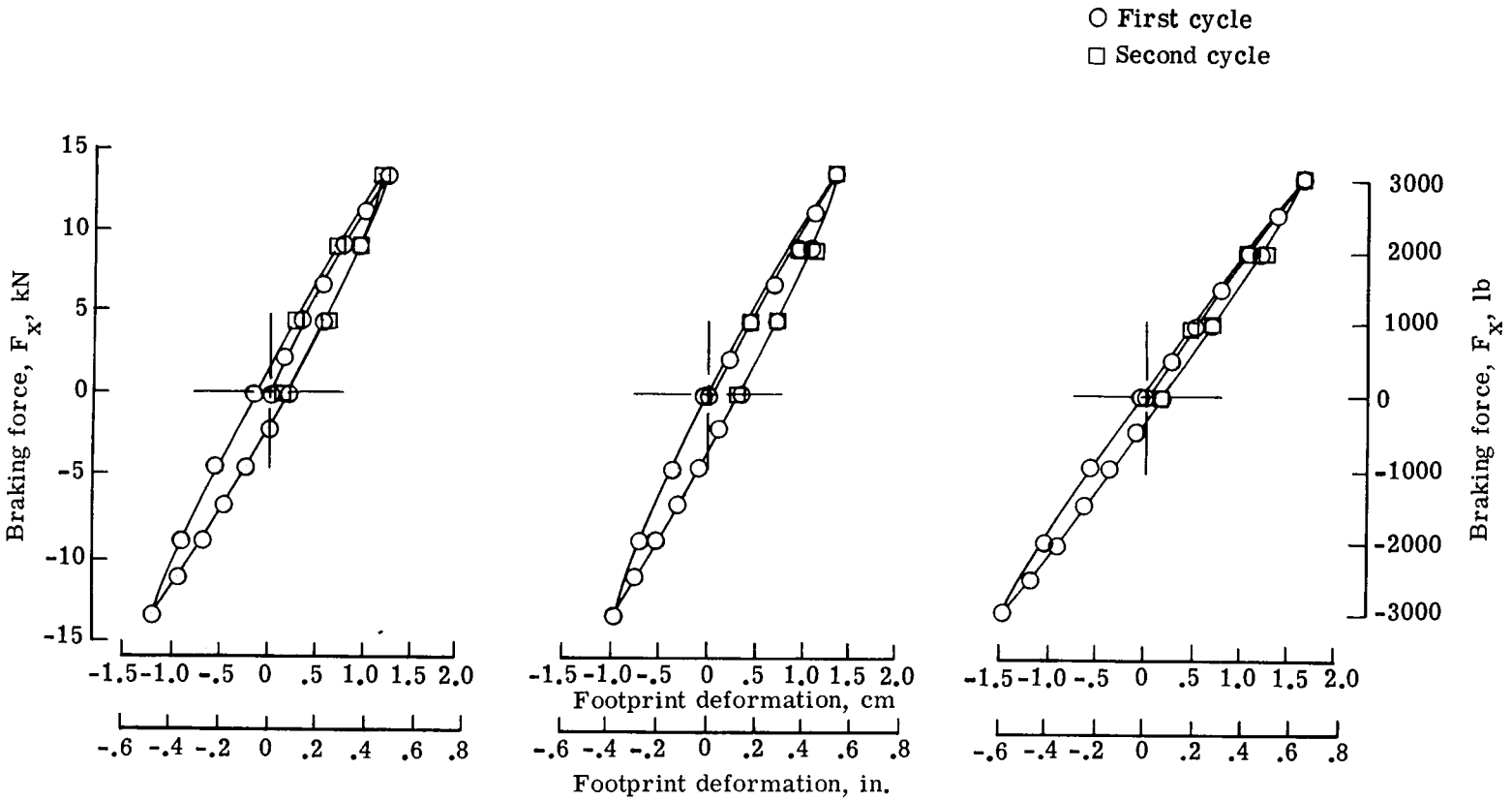

(a) Bias-ply tire. (b) Bias-belted tire. (c) Radial-belted tire.

Figure 9.- Typical static fore-and-aft load-deflection curves. F_z = 58.7 kN (13 200 lb); p = 793 kPa (115 lb/in^2).

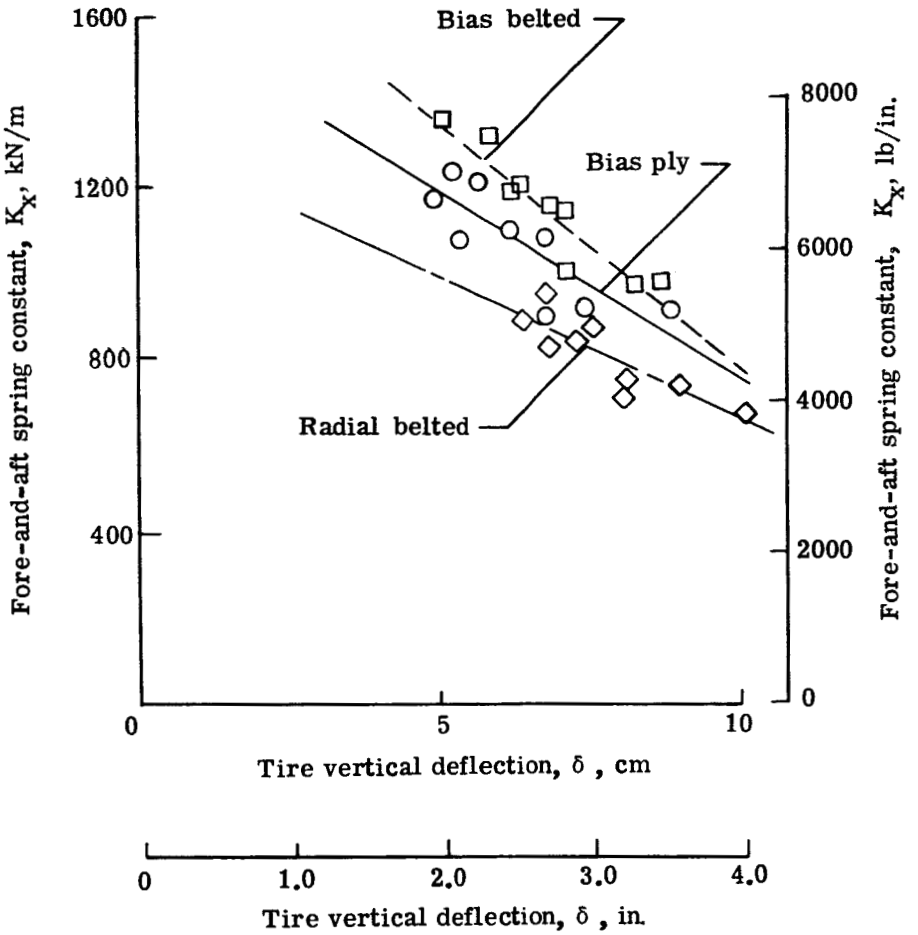

Figure 10.- Variation in fore-and-aft spring constant with tire vertical deflection.

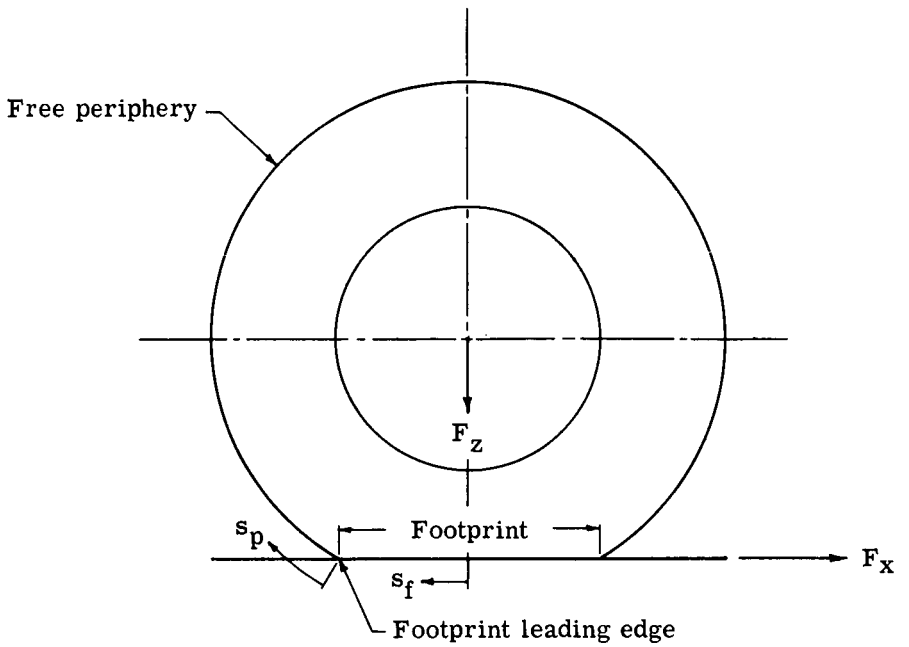

(a) Tire nomenclature.

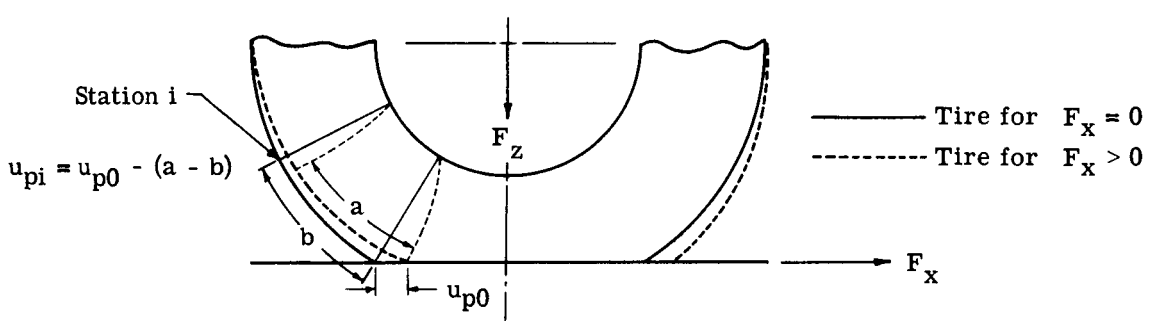

(b) Deformation in free periphery.

Figure 11.- Sketches illustrating tire nomenclature and deformation in free periphery under combined vertical load and braking force.

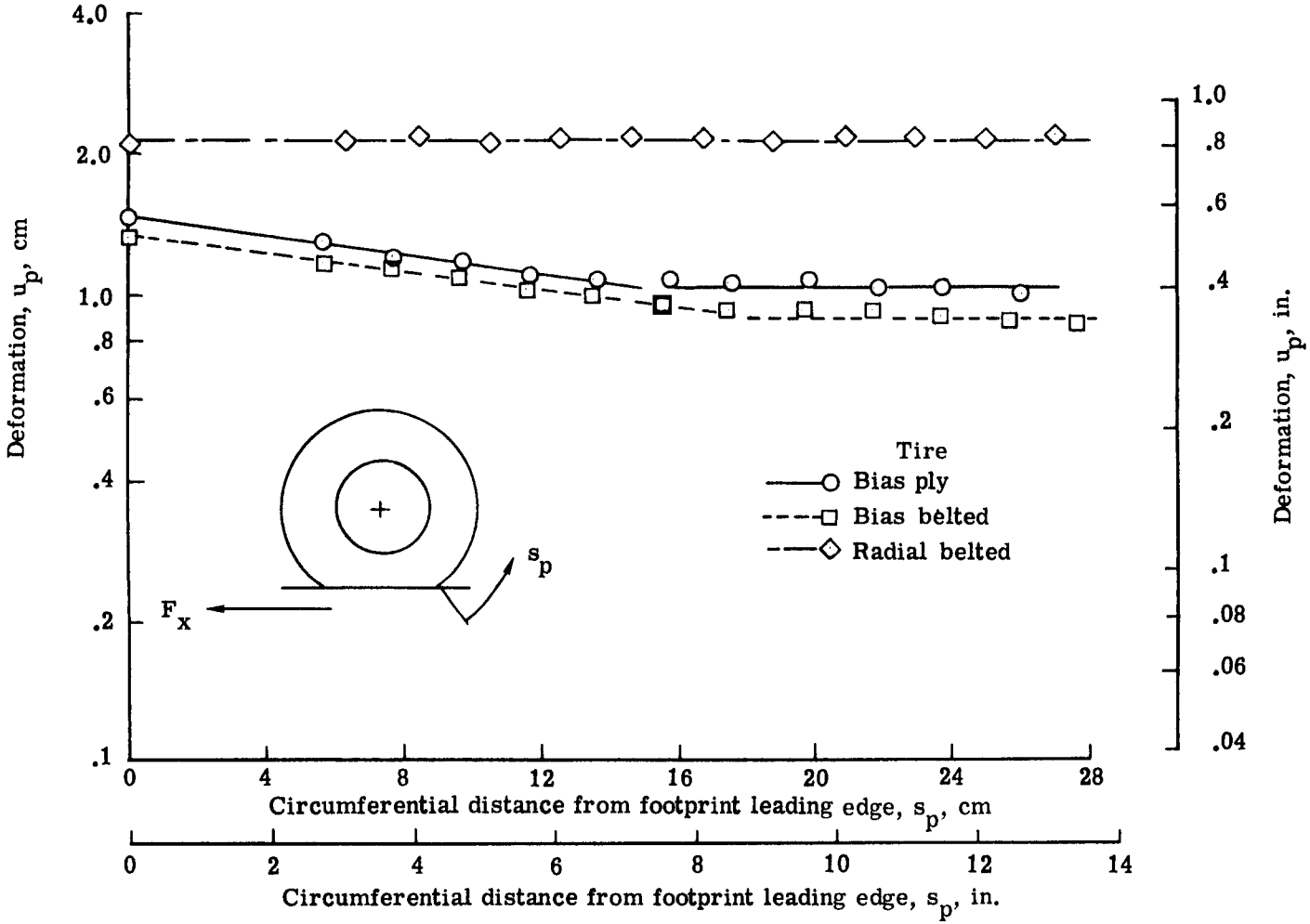

Figure 12.- Typical variation of deformations along free periphery under static-loading conditions. F_z = 66.8 kN (15 000 lb); p = 965 kPa (140 lb/in^2); F_x = 17.8 kN (4000 lb).

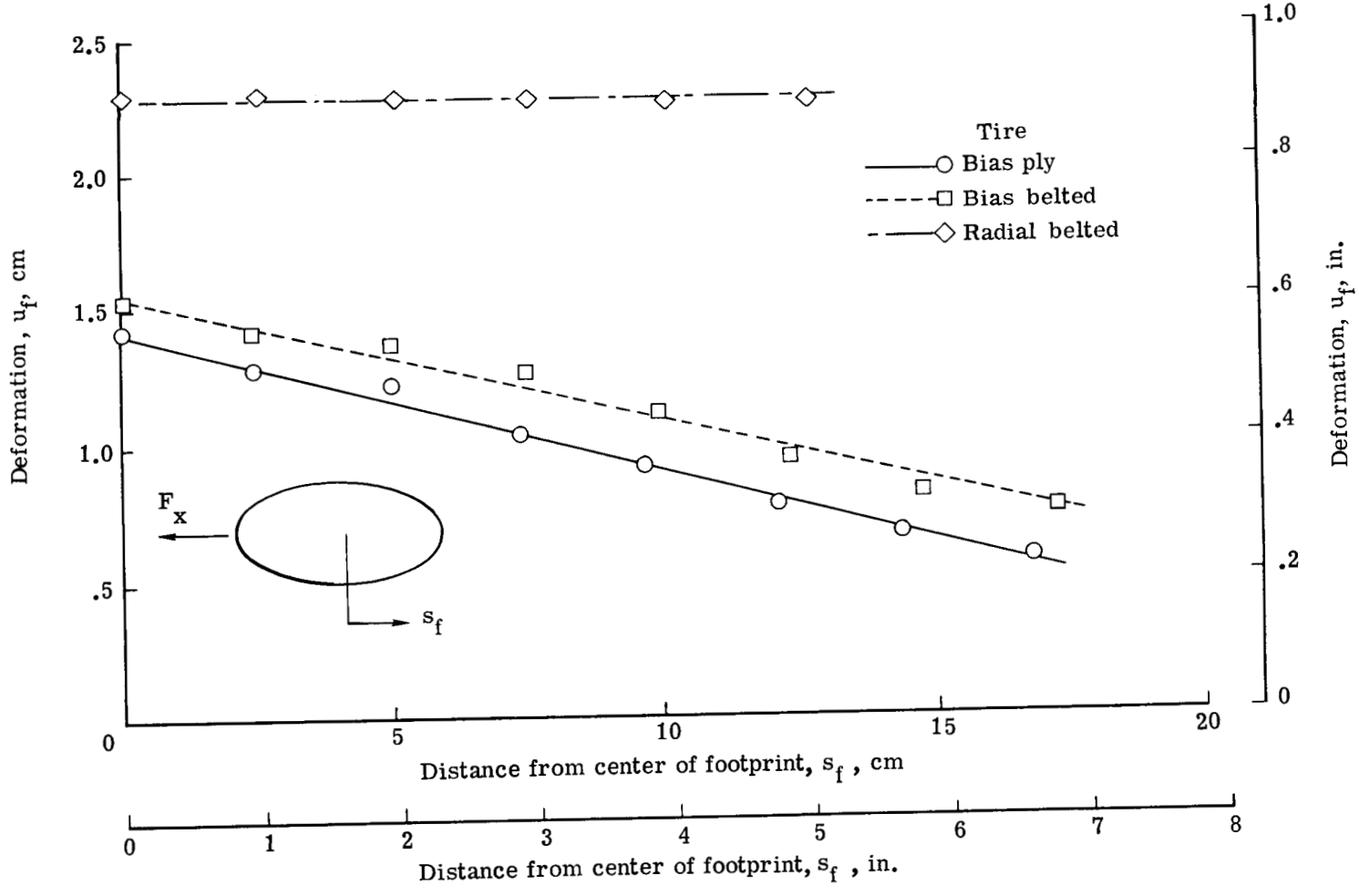

Figure 13.- Typical deformations within footprint for braked-rolling tests. F_Z = 66.8 kN (15 000 lb); p = 965 kPa (140 lb/in^2); $F_X \approx$ 17.8 kN (4000 lb).

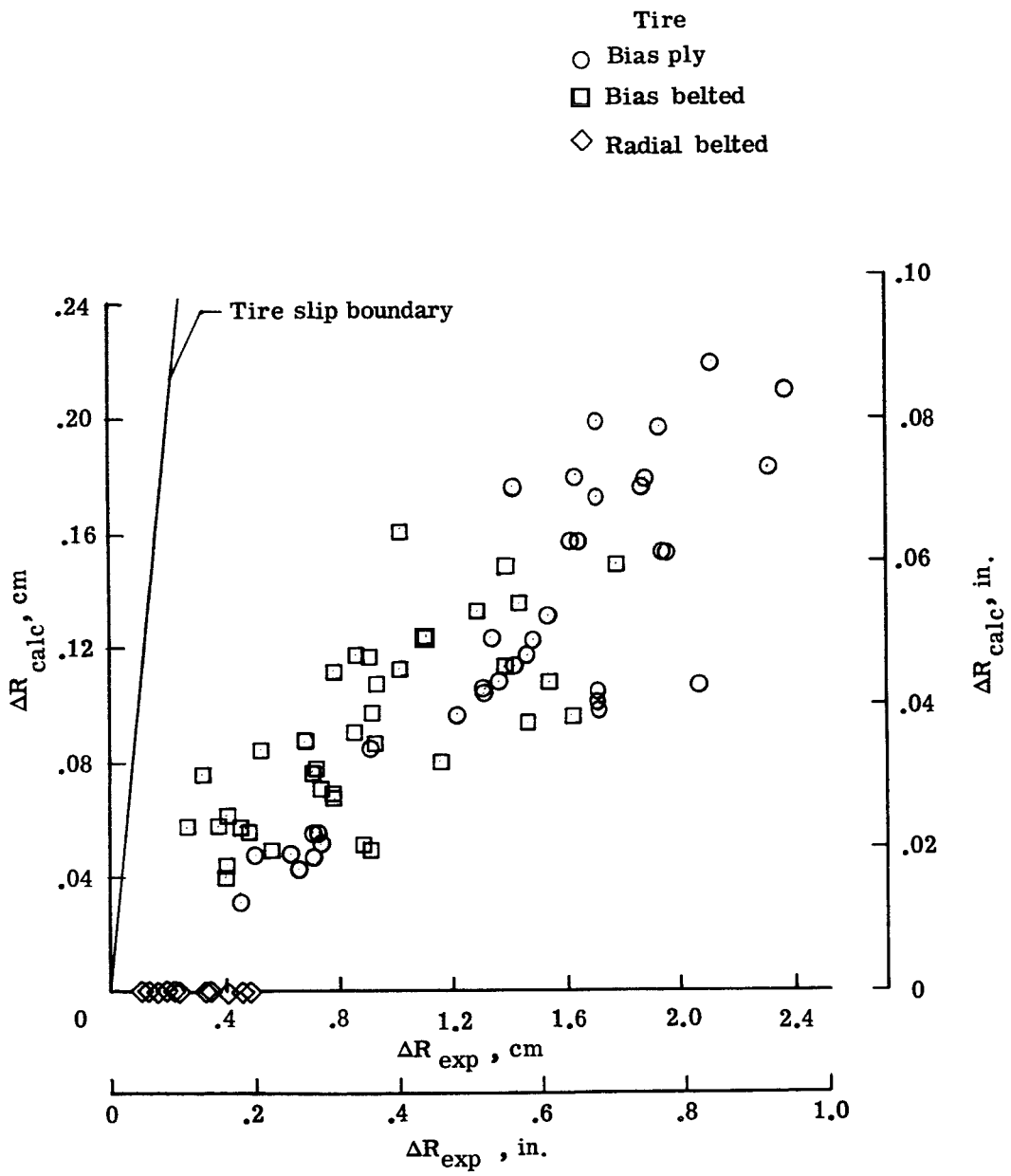

Figure 14.- Comparison of calculated and experimental change in rolling radius attributed to braking.

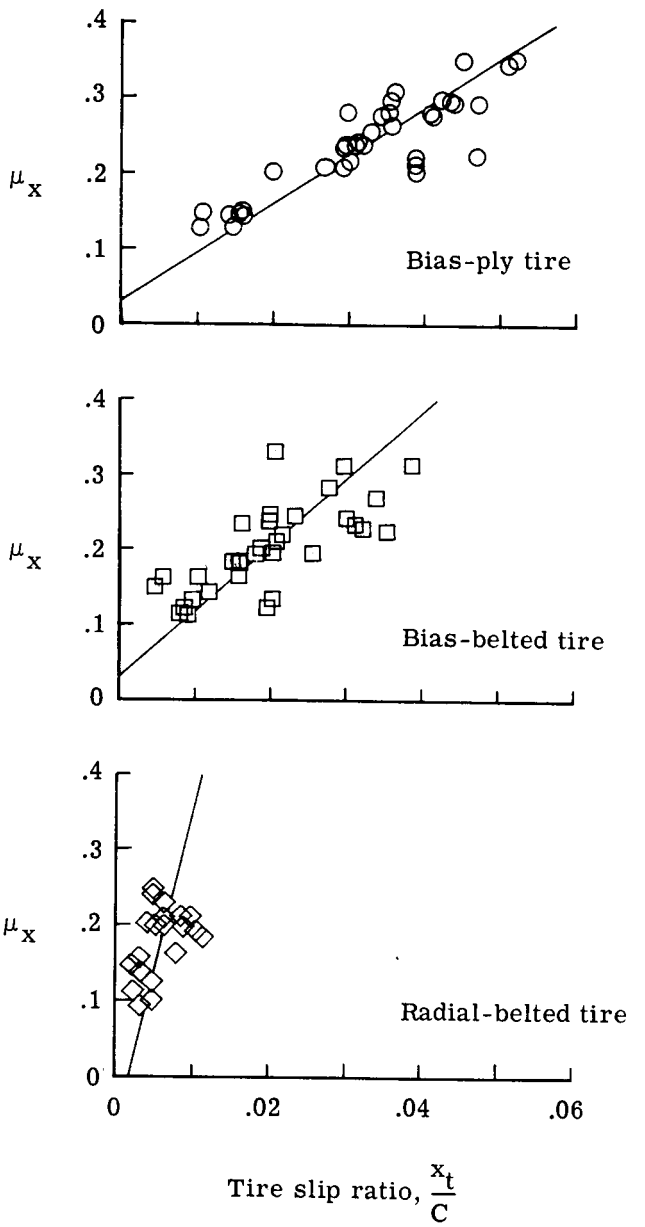

Figure 15.- Variation of braking friction coefficient with tire slip ratio.

For sale by the National Technical Information Service, Springfield, Virginia 22151

1. Report No.	2. Government Accession No.	3. Recipient's Catalog No.
NASA TN D-7449		

4. Title and Subtitle	5. Report Date
FORE-AND-AFT ELASTIC RESPONSE CHARACTERISTICS OF 34 × 9.9, TYPE VII, 14 PLY-RATING AIRCRAFT TIRES OF BIAS-PLY, BIAS-BELTED, AND RADIAL-BELTED DESIGN	April 1974
	6. Performing Organization Code

7. Author(s)	8. Performing Organization Report No.
John A. Tanner	L-8350
	10. Work Unit No. 501-38-12-02

9. Performing Organization Name and Address	11. Contract or Grant No.
NASA Langley Research Center Hampton, Va. 23605	
	13. Type of Report and Period Covered
12. Sponsoring Agency Name and Address	Technical Note
National Aeronautics and Space Administration Washington, D.C. 20546	14. Sponsoring Agency Code

15. Supplementary Notes

The information presented herein was offered as a thesis in partial fulfillment of the requirements for the degree of Master of Science, George Washington University, May 1973.

16. Abstract

An investigation was conducted to determined the fore-and-aft elastic response characteristics of 34 × 9.9, type VII, 14 ply-rating aircraft tires of bias-ply, bias-belted, and radial-belted design. The investigation consisted of static and rolling tests on dry concrete pavements at the Langley aircraft landing loads and traction facility; statistical techniques which related the measured tire elastic characteristics to variations in the vertical load, inflation pressure, braking force and/or tire vertical deflection; and a semiempirical analysis which related the tire elastic behavior to measured wheel slippage during steady-state braking.

The bias-belted tire developed the largest spring constant value for most loading conditions; the radial-belted tire, the smallest. The elastic response of the tire free periphery to static braking included both tread stretch and carcass torsional wind-up about the axle for the bias-ply and bias-belted tires and carcass wind-up alone for the radial-belted tire. Similarly, tread stretching under braked rolling conditions was detected within the footprints of the bias-ply and bias-belted tires but not within the footprint of the radial-belted tire. The tire slippage during steady-state braking was greater for the bias-ply tire than for the bias-belted and radial-belted tires.

17. Key Words (Suggested by Author(s))	18. Distribution Statement
Aircraft tire Elastic response Braking performance	Unclassified – Unlimited STAR Category 02

19. Security Classif. (of this report)	20. Security Classif. (of this page)	21. No. of Pages	22. Price
Unclassified	Unclassified	48	$3.25